TKK Dissertations 28
Espoo 2006

DIODE LASERS WITH OPTICAL FEEDBACK AND OPTICAL INJECTION

Applications in Metrology

Doctoral Dissertation

Markku Vainio

Helsinki University of Technology
Department of Electrical and Communications Engineering
Metrology Research Institute

TKK Dissertations 28
Espoo 2006

DIODE LASERS WITH OPTICAL FEEDBACK AND OPTICAL INJECTION

Applications in Metrology

Doctoral Dissertation

Markku Vainio

Dissertation for the degree of Doctor of Science in Technology to be presented with due permission of the Department of Electrical and Communications Engineering for public examination and debate in Auditorium S1 at Helsinki University of Technology (Espoo, Finland) on the 31st of March, 2006, at 12 noon.

Helsinki University of Technology
Department of Electrical and Communications Engineering
Metrology Research Institute

Teknillinen korkeakoulu
Sähkö- ja tietoliikennetekniikan osasto
Mittaustekniikka

Distribution:
Helsinki University of Technology
Department of Electrical and Communications Engineering
Metrology Research Institute
P.O. Box 3000
FI - 02015 TKK
FINLAND
URL: http://metrology.tkk.fi
Tel. +358-9-4511
Fax +358-9-451 2222
E-mail: markku.vainio@tkk.fi

© 2006 Markku Vainio

ISBN 951-22-8100-7
ISBN 951-22-8101-5 (PDF)
ISSN 1795-2239
ISSN 1795-4584 (PDF)
URL: http://lib.tkk.fi/Diss/2006/isbn9512281015/

TKK-DISS-2111

Picaset Oy
Helsinki 2006

HELSINKI UNIVERSITY OF TECHNOLOGY
P.O. BOX 1000, FI-02015 TKK
http://www.tkk.fi

ABSTRACT OF DOCTORAL DISSERTATION

Author Markku Vainio

Name of the dissertation

Diode Lasers with Optical Feedback and Optical Injection: Applications in Metrology

Date of manuscript

Date of the dissertation 31.3.2006

☐ Monograph

☑ Article dissertation (summary + original articles)

Department Electrical and Communications Engineering

Laboratory Metrology Research Institute

Field of research Measurement Science and Technology

Opponent(s) Dr. Leo Hollberg

Supervisor Prof. Erkki Ikonen

(Instructor) Dr. Mikko Merimaa

Abstract

The visible red near 633 nm is an important spectral region in length metrology. Iodine-stabilized He-Ne (HeNe/I2) laser stabilized on the hyperfine spectrum of the R(127)11-5 transition is one of the most used optical frequency standards for practical realization of the definition of the meter. Furthermore, the existence of much stronger transitions in the vicinity of R(127)11-5 motivates to develop new frequency standards based on tunable diode lasers. Both to improve already existing optical frequency standards and to develop new ones, precise absolute frequency measurements of the used iodine transitions are needed. At present, such measurements can be performed using an optical femtosecond frequency comb generator. In this thesis, diode laser systems for absolute frequency measurements with the optical frequency comb generator have been developed. In order to improve diode laser performance to the required level, optical feedback and optical injection locking techniques have been used.

To facilitate the absolute frequency measurements of the HeNe/I2 laser, an optical amplifier has been constructed. The amplifier can be reliably operated over several hours with very low phase noise, and it has been successfully used in absolute frequency determination of an iodine-stabilized He-Ne laser. For absolute frequency determination of various iodine transitions in the vicinity of 633 nm, a laser spectrometer has been realized. The new spectrometer design has been made particularly for good frequency accuracy and reproducibility. It combines, through injection locking, good beam quality of a microlens-coupled diode laser with high spectral quality of a stable external-cavity diode laser. The spectrometer uses wavelength modulation technique for locking the laser frequency to an iodine hyperfine component. For this reason, the modulation transfer properties of injection-locked diode lasers have been investigated in detail. In particular, suppression of intensity modulation and reproduction of frequency modulation have been considered, for the first time, in terms of master-slave frequency detuning. Also the conversion of the master laser frequency modulation into slave laser intensity modulation has been considered. In addition to spectroscopy, the results are useful in optical communications.

Keywords Diode lasers, external cavity, injection locking, optical frequency measurements, frequency comb

ISBN (printed) 951-22-8100-7 | ISSN (printed) 1795-2239

ISBN (pdf) 951-22-8101-5 | ISSN (pdf) 1795-4584

ISBN (others) | Number of pages 57 + 41

Publisher Helsinki University of Technology, Metrology Research Institute

Print distribution Helsinki University of Technology, Metrology Research Institute

☑ The dissertation can be read at http://lib.tkk.fi/Diss/ 2006/isbn9512281015/

TEKNILLINEN KORKEAKOULU PL 1000, 02015 TKK http://www.tkk.fi	VÄITÖSKIRJAN TIIVISTELMÄ

Tekijä Markku Vainio

Väitöskirjan nimi

Optista takaisinkytkentää ja optista injektiota hyödyntävät diodilaserit: sovellukset metrologiassa

Käsikirjoituksen jättämispäivämäärä	Väitöstilaisuuden ajankohta 31.3.2006
☐ Monografia	☒ Yhdistelmäväitöskirja (yhteenveto + erillisartikkelit)

Osasto Sähkö- ja tietoliikennetekniikan osasto
Laboratorio MIKES TKK Mittaustekniikka
Tutkimusala Mittaustekniikka
Vastaväittäjä(t) Dr. Leo Hollberg
Työn valvoja Prof. Erkki Ikonen
(Työn ohjaaja) TkT Mikko Merimaa

Tiivistelmä

Eräs tärkeimmistä pituusmetrologiassa käytetyistä aallonpituusalueista on näkyvän punaisen valon alue. Esimerkkinä voidaan mainita jodin R(127)11-5 absorptioviivan ylihienorakenteeseen stabiloitu 633 nm helium-neonlaser (HeNe-laser), joka on yksi suosituimmista metrin määritelmän käytännön realisointiin käytetyistä optisista taajuusstandardeista. Jodimolekyylillä on absorptioviivan R(127)11-5 läheisyydessä myös muita paljon voimakkaampia viivoja, mikä osaltaan kannustaa kehittämään uusia, säädettäviin puolijohdelasereihin perustuvia taajuusstandardeja. Jodin absorptio-viivojen tarkkoja taajuusmittauksia tarvitaankin sekä vanhojen jo olemassa olevien taajuusstandardien parantamiseen, että kokonaan uusien taajuusstandardien kehittämiseen. Nykyisin kyseisiä taajuusmittauksia voidaan tehdä optisen taajuuskampageneraattorin avulla. Tässä väitöskirjassa on tutkittu ja kehitetty diodilaserlaitteistoja joita voidaan käyttää optisiin absoluuttitaajuusmittauksiin yhdessä taajuuskampageneraattorin kanssa. Diodilasereiden ominaisuuksia on parannettu mittauksissa vaadittavalle tasolle käyttäen hyväksi optiseen takaisinkytkentään ja injektiolukitukseen perustuvia tekniikoita.

Osana väitöskirjatyötä on rakennettu injektiolukitukseen perustuva optinen vahvistin, jonka avulla voidaan helpottaa ja yksinkertaistaa HeNe-lasereiden taajuusmittauksia. Vahvistinta on onnistuneesti käytetty jodistabiloidun HeNe-laserin absoluuttisen taajuuden määrittämiseen taajuuskampatekniikalla. Lisäksi työssä on kehitetty diodilaseriin perustuva laserspektrometri, jolla on mahdollista mitata useiden eri jodiviivojen absoluuttiset taajuudet 633 nm aallonpituuden ympäristössä. Uuden spektrometrin suunnittelussa on kiinnitetty erityistä huomiota hyvään taajuustarkkuuteen ja -toistettavuuteen. Spektrometrissä on hyödynnetty injektiolukitustekniikkaa, jonka avulla on voitu yhdistää mikro-linssillä varustetun diodilaserin ulostulosäteen hyvä spatiaalinen laatu toisen, voimakkaaseen optiseen takaisin-kytkentään perustuvan diodilaserin hyviin taajuusominaisuuksiin. Lasertaajuus lukitaan tarkasteltavaan jodin ylihieno-rakennekomponenttiin aallonpituusmodulaatioon perustuvaa tekniikkaa käyttäen. Tästä syystä väitöskirjassa on tutkittu myös sitä kuinka eri modulaatiosignaalit siirtyvät ns. päälaserista (master) injektiolukittuun diodilaseriin (slave). Erityisesti on tarkasteltu intensiteettimodulaation vaimenemista ja taajuusmodulaation toistumista injektio-lukituksessa käytettyjen lasereiden taajuuseron suhteen. Saatuja tuloksia voidaan hyödyntää spektroskopian lisäksi mm. optisessa tietoliikenteessä.

Asiasanat diodilaser, injektiolukitus, optiset taajuusmittaukset, taajuuskampa

ISBN (painettu) 951-22-8100-7	ISSN (painettu) 1795-2239
ISBN (pdf) 951-22-8101-5	ISSN (pdf) 1795-4584
ISBN (muut)	Sivumäärä 57 + 41

Julkaisija Teknillinen korkeakoulu , MIKES TKK Mittaustekniikka

Painetun väitöskirjan jakelu Teknillinen korkeakoulu , MIKES TKK Mittaustekniikka

☒ Luettavissa verkossa osoitteessa http://lib.tkk.fi/Diss/2006/isbn9512281015/

PREFACE

The research work presented in this thesis has been carried out at the Metrology Research Institute, Department of Electrical and Communications Engineering of the Helsinki University of Technology, during the years 2002 – 2005.

I wish to express my gratitude to Professor Pekka Wallin, the Head of the Department of Electrical and Communications Engineering, for providing the opportunity to work in the interesting field of metrology. I also want to express my gratitude to my supervisor, Professor Erkki Ikonen, for valuable guidance during the work.

I am very grateful to my instructor, Dr. Mikko Merimaa, for encouragement, advices and helpful discussions throughout this research. I also want to thank all the co-authors of the publications, as well as the colleagues at the Metrology Research Institute for their contribution to the thesis, and for creating an inspiring working atmosphere. Especially the help by Dr. Kaj Nyholm with the experiments and writing of papers is acknowledged.

The financial support by the Emil Aaltonen Foundation, the Finnish Cultural Foundation, the Finnish Academy of Science and Letters (Väisälän rahasto), and Graduate School of Electrical and Communications Engineering is greatly appreciated.

Finally, I want to express my sincere gratitude to my family and friends for their support throughout my studies.

Espoo, March 2006

Markku Vainio

LIST OF PUBLICATIONS

This thesis consists of an overview and the following selection of the author's publications.

I. M. Vainio, M. Merimaa, Y. Sidorin, M. Kuittinen, and E. Ikonen, "*Miniaturized Transmission Grating Laser at 1.55 μm with 128 nm Tuning Range*," IEEE Photonics Technology Letters, Vol. **15**, No. 7, pp. 990-992 (2003).

II. M. Vainio, M. Merimaa, and E. Ikonen, "*Iodine spectrometer based on a 633-nm transmission-grating diode laser*," Meas. Sci. Technol., Vol. **16**, No. 6, pp. 1305-1311 (2005).

III. M. Vainio, M. Merimaa, and K. Nyholm, "*Modulation transfer characteristics of injection-locked diode lasers,*" Metrology Research Institute Report **29/2005**, 14 pages.

IV. M. Vainio, M. Merimaa, and K. Nyholm, "*Optical amplifier for femtosecond frequency comb measurements near 633 nm*," Appl. Phys. B, Vol. **81**, No. 8, pp. 1053-1057 (2005).

V. M. Merimaa, K. Nyholm, and M. Vainio, "*MIKES frequency comb generator and absolute frequency measurements of iodine-stabilized lasers,"* Proc. of 12th Int. Conf. on Metrology, June 20–23, 2005, Lyon, France (2005), 6 pages.

AUTHOR'S CONTRIBUTION

The research work presented in this thesis has been carried out at the Metrology Research Institute (MRI) during the years 2002 – 2005. The thesis consists of a short overview and six publications that are listed on the previous page. All publications are the results of group effort. The author has prepared the manuscripts of Publications I–IV, and contributed to the writing of Publication V.

The author has designed the experimental setups presented in Publications II–IV and constructed the lasers and setups of Publications I–IV. He has also designed and built part of the electronics needed in the experiments. The author is responsible for the theoretical model and results of Publication III. Most of the measurements and experiments described in Publications I–IV have been performed by the author. He has also contributed to the measurements and construction of the equipment of Publication V.

CONTENTS

ABSTRACT **3**

PREFACE **7**

LIST OF PUBLICATIONS **8**

AUTHOR'S CONTRIBUTION **9**

CONTENTS **10**

1. INTRODUCTION **11**

1.1. BACKGROUND 11
1.2. THESIS OUTLINE 12

2. THEORY **14**

2.1. DIODE LASER CHARACTERISTICS 14
2.1.1. Threshold condition and rate equations *15*
2.1.2. Linewidth enhancement factor *16*
2.1.3. Frequency noise and linewidth *17*
2.1.4. Intensity noise *20*
2.1.5. Spectrum and wavelength tuning *21*
2.2. DIODE LASERS WITH OPTICAL FEEDBACK 22
2.2.1. Strong optical feedback *22*
2.3. DIODE LASERS WITH OPTICAL INJECTION 26
2.4. DOPPLER-FREE SPECTROSCOPY OF MOLECULAR IODINE 29
2.4.1. Iodine as a frequency reference *29*
2.4.2. Line broadening and saturation spectroscopy *30*
2.4.3. Frequency shifts in iodine *34*

3. EXTERNAL-CAVITY DIODE LASERS **35**

3.1. 1550-NM TRANSMISSION-GRATING DIODE LASER 36
3.2. 633-NM TRANSMISSION-GRATING DIODE LASER 38
3.2.1. Modulation characteristics *39*

4. INJECTION-LOCKED DIODE LASER SYSTEMS **40**

4.2. IODINE SPECTROMETER 40
4.3. MODULATION TRANSFER IN DIODE LASER INJECTION LOCKING 41
4.4. OPTICAL AMPLIFIER 45

5. OPTICAL FREQUENCY COMB **47**

6. CONCLUSION **50**

REFERENCES **52**

1. INTRODUCTION

1.1. Background

Semiconductor diode lasers are currently the most used lasers in optical telecommunications, atom physics, and spectroscopy. For these applications diode lasers offer an attractive combination of compactness, reliability, tunability, good efficiency, and low price. They have low intensity noise and their frequency and intensity can be modulated at high frequencies by direct modulation of the injection current. Diode lasers are available at several spectral regions from blue to far infrared, with output powers ranging from few milliwatts up to several watts of broad-area diode lasers.

Spectral linewidth of a solitary diode laser is typically several MHz or more, and thus too large for many applications. The use of diode lasers e.g. in spectroscopy is impeded also due to longitudinal mode hopping when tuning the wavelength. An extensively used technique to improve spectral properties of a diode laser is to subject it to strong and frequency selective optical feedback from an external grating (Fig. 1.1) [1,2]. In this way the instantaneous linewidth can be narrowed even down to kilohertz-level. Such external cavity diode laser (ECDL) with an antireflection (AR) coated diode output facet also provides an easy way for mode-hop free tuning of the laser wavelength, making an ideal tool for spectroscopy.

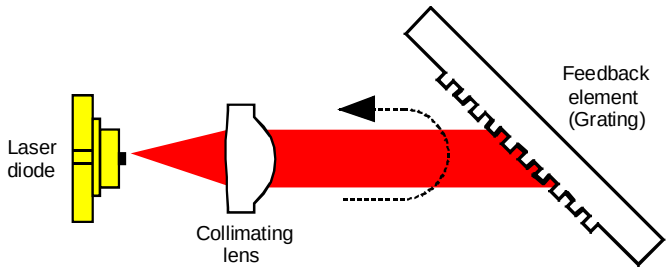

Fig. 1.1 *Principle of external-cavity diode laser. Linewidth of a solitary diode laser is narrowed due to strong optical feedback from an external reflector, typically a grating. Laser wavelength can be tuned by rotating the grating.*

Despite the several benefits of the ECDLs they have some limitations, too. For example, in spectroscopy or nonlinear optics the poor beam quality and relatively small output power of most ECDLs can be troublesome. Even more severe limitations often result from the ECDLs' sensitivity to mechanical vibrations and ambient temperature and pressure variations. If careful design of the ECDL and minimization of these effects does not provide high enough stability, the laser frequency can be locked to a more stable frequency reference, such as an optical resonator or a molecular transition.

Another commonly used method to improve spectral purity of a diode laser (or to amplify the output power of a narrow-linewidth diode laser) is injection locking. Light from a master laser with desired spectral properties is injected into a slave laser that will, in certain conditions, lock to the frequency of the master laser. Just as the various effects of optical feedback, diode laser injection locking has been extensively studied both theoretically and experimentally [3,4]. In addition to laser synchronization, diode laser injection locking has been demonstrated to provide enhanced modulation bandwidth [5,6], reduced frequency chirping [7], and reduced sensitivity to detrimental optical feedback [8], for instance.

1.2. Thesis outline

The main goal of the research summarized in this thesis has been to develop techniques based on optical feedback and optical injection in order to improve diode laser characteristics to make them better suited for applications of spectroscopy and length metrology.

In Chapter 2, the theory related to this thesis is reviewed. First, the diode laser characteristics and in particular the spectral properties are considered, together with the effects of external optical feedback and optical injection. Secondly, saturation spectroscopy and the properties of iodine ($^{127}I_2$) as a frequency reference are briefly discussed.

In Chapter 3, the constructed external-cavity diode lasers are presented. The lasers utilize transmission grating [9] as the optical feedback element. The transmission-grating geometry allows a simple, compact, and robust laser structure with invariant output beam pointing. Transmission grating has been shown to give reliable operation over the entire gain spectra of the used diode lasers. For example, at telecommunication wavelengths, a tuning range as wide as 128 nm has been demonstrated [Publ. I]. Also, a new transmission-grating laser design with very good passive stability at 633 nm wavelength has been realized [Publ. II]. The good frequency reproducibility and narrow linewidth of 450 kHz (for 1 s integration time) make the laser ideal for many applications in metrology and atom optics.

In Chapter 4, the developed techniques and apparatuses based on diode laser injection locking are introduced. Especially in frequency modulation spectroscopy and optical communication the modulation characteristics of the laser system are of importance. Moreover, the use of injection locking for improving laser operation in these applications has recently gained a lot of interest. For these reasons, a detailed study on the modulation transfer properties of injection locked diode lasers has been performed [Publ. III]. In particular, suppression of intensity modulation and reproduction of frequency modulation have been considered, for the first time, in terms of master-slave detuning. The presented results are of practical importance in designing of injection-locked diode laser systems that utilize frequency modulation or intensity modulation.

Chapter 4 also summarizes the work done on two applications where diode laser injection locking has been successfully used. First, an iodine spectrometer setup is presented [Publ. II]. The novel design has been made particularly for good frequency accuracy and reproducibility, and it is intended for absolute frequency measurements of various iodine absorption lines in the vicinity of 633 nm. Such measurements are needed to improve the frequency standards based on iodine-stabilized lasers. The realization based on injection locking makes the system less sensitive to optical feedback, and combines good beam quality of a microlens-coupled diode laser with high spectral quality of an external-cavity diode laser. The use of injection locking also reduces spurious intensity modulation associated with direct current modulation of the ECDL, thus allowing much higher modulation frequencies than the conventionally used method where modulation is made using a piezoelectric transducer (PZT).

Another presented application of injection locking is an optical amplifier, which is used to amplify the output of an iodine-stabilized He-Ne laser [Publ. IV]. Iodine-stabilized He-Ne laser at 633 nm is the most widely used optical frequency standard for the practical realization of the definition of the meter [10], and commonly used e.g. in frequency calibration of lasers used in length measurements. To use a laser as a

frequency standard, its absolute frequency must be determined. The establishment of the femtosecond frequency comb technology [11] has made such measurements available to many national measurement institutes, thus allowing them to improve their calibration facilities. This means increased demand for absolute frequency measurements of the frequency standard lasers, such as the He-Ne lasers. Unfortunately, however, the output power of the iodine-stabilized He-Ne laser is too low for direct frequency comb measurements. The amplifier described here provides a convenient and inexpensive all-optical way to amplify the laser output to the level required for reliable beat frequency counting, thus greatly improving and simplifying the measurements. The detailed system description and characterization allows other laboratories to directly implement similar approach to their measurement setups, too.

In Chapter 5, the femtosecond frequency comb technology is outlined. In particular, the MIKES* frequency comb used in the absolute frequency measurements referred in this thesis is discussed [Publ. V]. The frequency comb technology is currently used in many laboratories to measure e.g. the values of fundamental physical constants or frequencies of stabilized lasers. It allows direct optical frequency measurements against a primary frequency standard without loss of accuracy, hence providing substantial improvement compared to previously used frequency chains that are extremely complicated and laborious to use. In addition to the description of the MIKES frequency comb generator, Publication V reports the results of absolute frequency determination of iodine-stabilized Nd:YAG laser at 532 nm and He-Ne laser at 633 nm. The measured frequencies are in very good agreement with previous results and the CIPM† recommended values, the measured frequency differences being less than 0.2 kHz for the most important $^{127}I_2$ transitions.

* MIKES = Centre for Metrology and Accreditation, Finland.
† Comité International des Poids et Mesures (International Committee for Weights and Measures)

2. THEORY

2.1. Diode laser characteristics

Just like any oscillator, a laser needs both gain and feedback in order to work. To reach the lasing threshold, the gain must overcome the losses of the system. In diode lasers, the optical gain is obtained by passing current trough the active region, and the feedback is provided by the diode facets that form the resonator. The facets are made by cleaving, and their reflectivity may be further tailored using suitable coatings. Due to the high gain of typical diode laser active materials, the laser cavity can be made very short. Typical values for the cavity length are between 100 μm and 1 mm♣.

Even if the longitudinal mode spacing of diode lasers is typically large, simple structures have a tendency to oscillate in multiple longitudinal modes. This is due to the large gain bandwidth of the semiconductor materials. For example, at telecommunication wavelengths in the 1.5-μm spectral region, InGaAsP laser operation over a bandwidth as large as 240 nm has been demonstrated [12,13]. For the InGaAlP devices operating in visible red, a typical gain bandwidth is 5 to 15 nm. In addition to the used semiconductor material, the position and width of the gain band depends on the structure of the laser diode. Present laser diodes are fabricated with heterostructures for low thresholds and continuous wave operation in room temperature. The heterostructure widths can be chosen to produce either a bulk or a more advanced quantum-well gain medium.

Lateral confinement of the laser field is achieved by gain guiding or index guiding, with various designs introduced [14,15]. In a gain-guided device the lateral extent of the laser field is controlled by injection current distribution and in an index-guided device by an optical waveguide that is formed by suitably structured refractive index profile. The geometry of the active layer may be designed for different purposes, e.g. using narrow stripes for single transverse-mode operation, or broad active regions for high output power. The active region is typically a few micrometers wide, while the thickness is much smaller, for the quantum well structures only a few nanometers. This leads to highly diverging and asymmetric (elliptical) output beam. In addition to a collimating lens, reshaping optics or spatial filtering is needed for some applications where a Gaussian beam profile is desirable.

General properties and practical details of diode lasers are covered in more detail e.g. in reference [1] and the related material physics in [16]. In the following, some of the most essential properties are reviewed. For the two applications considered in this work, spectroscopy and amplification of a frequency standard laser, good spectral purity and stability are perhaps the most important requirements for the used diode lasers. For that reason, the diode laser spectral properties are discussed in more detail.

♣ Here only edge emitting lasers are considered. Another type of diode laser, VCSEL (vertical cavity surface emitting laser) emits light in a direction perpendicular to the semiconductor wafer on which it has been fabricated. In such structure the cavity length is typically of the same order of magnitude as the emitted wavelength.

2.1.1. Threshold condition and rate equations

The diode laser threshold gain can be estimated from the unity round-trip condition for intensity in a Fabry-Pérot cavity

$$R_1 R_2 e^{2(g_{th}-\alpha_m)L} = 1, \tag{2.1}$$

where R_1 and R_2 are the power reflectivities of the front and rear facets of the laser diode, respectively. The laser cavity length is given by L, and α_m accounts for the internal optical losses. Solving Eq. (2.1) for the threshold gain per unit length gives

$$g_{th} = \alpha_m - \frac{\ln(R_1 R_2)}{2L}. \tag{2.2}$$

The gain per unit length is converted to gain per unit time (G) by multiplying with $v_g = c/n$, with c being the vacuum speed of light and n denoting the real part of the refractive index.

Dynamic behavior, such as the modulation characteristics, of diode lasers are commonly modeled using the following rate equations for the cavity photon number S, phase ϕ, and carrier density N. Derivation of the diode laser rate equations is given e.g. in references [3,17].

$$\frac{dS(t)}{dt} = \left(G(N) - \frac{1}{\tau_p} \right) S(t) + R_{sp} + F_S(t) \tag{2.3.a}$$

$$\frac{d\phi(t)}{dt} = \frac{\alpha}{2} \left(G(N) - \frac{1}{\tau_p} \right) + F_\phi(t) \tag{2.3.b}$$

$$\frac{dN(t)}{dt} = \frac{I(t)}{e} - \frac{N(t)}{\tau_N} - G(N)S(t) + F_N(t), \tag{2.3.c}$$

where $I(t)$ denotes the laser injection current, e is the electron charge, τ_N is the carrier lifetime, τ_p is the photon lifetime, α is the linewidth enhancement factor, and $G(N)$ is the modal gain per unit time. R_{sp} is the spontaneous emission rate and $F_S(t)$, $F_\phi(t)$, and $F_N(t)$ are the Langevin noise terms [18] for the photon number, phase, and carrier density, respectively. Spectral hole burning and other effects leading to gain compression are neglected and the gain is assumed to be a linear function of the carrier density N

$$G(N) = G_0(N - N_{tr}) = A_g \Gamma (N - N_{tr}), \tag{2.4}$$

where G_0 is the gain coefficient and A_g is the differential gain. Confinement factor Γ describes the overlapping between the lasing mode and the active region. Carrier number for transparency (or zero gain) is denoted by N_{tr}.

The photon lifetime τ_p depends on the cavity losses as

$$\tau_p = \frac{n}{c} \left[\alpha_m - \frac{\ln(R_1 R_2)}{2L} \right]^{-1}. \tag{2.5}$$

Using this relation together with Eq. (2.2) we can write the gain at the threshold as

$$G(N_{th}) = \frac{1}{\tau_p}, \tag{2.6}$$

which allows us to express the rate equations in the following form that will be used later on in this thesis

$$\frac{dS(t)}{dt} = G_0\left(N(t) - N_{th}\right)S(t) \tag{2.7.a}$$

$$\frac{d\phi(t)}{dt} = \frac{\alpha}{2}G_0\left(N(t) - N_{th}\right) \tag{2.7.b}$$

$$\frac{dN(t)}{dt} = \frac{I(t)}{e} - \frac{N(t)}{\tau_N} - G_0\left(N(t) - N_{tr}\right). \tag{2.7.c}$$

For simplicity, the terms describing the spontaneous emission and noise are omitted.

Static behavior of the laser can be found from the stationary solutions of the rate equations, i.e. by setting the time derivatives dS/dt, $d\phi/dt$, and dN/dt to zero. Above the laser threshold the carrier density N is clamped at the threshold value N_{th}, while the laser power increases linearly with the injection current I. The corresponding slope describes the laser current-to-light efficiency i.e. the differential efficiency (or slope efficiency), which is given in W/A. Laser output power through the front facet may be calculated from the cavity photon number S using

$$P_{out} = \frac{c}{2nL}\ln\left(\frac{1}{R_1}\right)Sh\nu\,, \tag{2.8}$$

where the photon energy is given as a product of the Planck constant $h = 6.626\times10^{-34}$ Js and the emitted optical frequency ν.

2.1.2. Linewidth enhancement factor

In most lasers, the laser transition occurs between two discrete energy levels and the gain curve is symmetric around its maximum value. The refractive index dispersion curve is also symmetric and has a zero at the frequency of the maximum gain, as is demonstrated in Fig. 2.1 a. The gain (or imaginary part of the refractive index) and (the real part of) the refractive index are coupled together via the Kramers-Kronig dispersion relations [19].

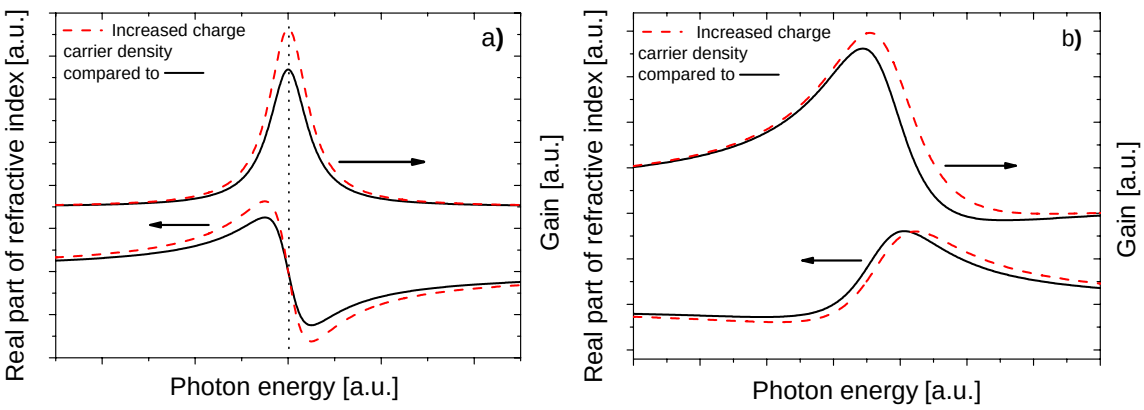

Fig. 2.1 *In case of symmetric gain and refractive index dispersion curves (a) the coupling of phase and intensity near the gain maximum is negligible, while in semiconductor lasers the asymmetric gain (b) leads to stronger coupling and thus (via carrier density variations) to significant line broadening. Curves in (a) have been calculated from the Kramers-Kronig relations [19] and (b) has been calculated according to the model introduced in Ref. [20].*

Contrary to many other laser types, in diode lasers the lasing transition takes place between two energy bands, which leads to a shift of the refractive index dispersion curve relative to the gain curve (Fig. 2.5 b). This is because of the asymmetry of the gain curve. The asymmetry is for the reason that the gain material is transparent at long wavelengths where the photon energy is below the bandgap, while higher energy photons are strongly absorbed [21]. As the gain changes with carrier density, also the refractive index around the lasing frequency is dependent on the carrier density. The coupling between carrier-concentration induced variations of the real and imaginary parts of the refractive index is commonly described using the linewidth enhancement factor (or antiguiding parameter) α, which is defined as [22]

$$\alpha = -2k \frac{dn/dN}{dg/dN}. \tag{2.9}$$

Above k is the free-space wave vector, n is the real part of the refractive index, and g is the gain per unit length. The linewidth enhancement factor is typically between 2 and 10, but is dependent e.g. on photon energy, temperature, material parameters, and laser structure. For example, quantum well structure can be used to reduce the value of α. Another way is to force the laser to operate on the short wavelength side of the gain curve, e.g. by using an external cavity with a frequency selective component [21,23]. The linewidth enhancement factor is an important parameter not only because it has a significant effect on the spectral properties of a solitary diode laser but also because it has a major contribution on how the laser behaves under optical feedback and optical injection. Therefore, various experimental methods have been developed to determine the linewidth enhancement factor [22]. In practice, however, the actual value for a given laser component is usually not very precisely known. (The same applies to most of the diode laser internal parameters). In the theoretical calculations presented in this thesis the values for the linewidth enhancement factor are selected to support the experimental observations. The aforementioned dependencies on temperature etc. are omitted.

2.1.3. Frequency noise and linewidth

The fundamental, or inherent, linewidth is caused essentially by altering of phase due to fluctuations caused by spontaneous emission. This is illustrated in Fig. 2.2, where the electric field of a single mode laser is given by

$$E(t) = \left[E_0 + \Delta E(t)\right] e^{\mathrm{j}(2\pi\nu + \Delta\phi(t))}, \tag{2.10}$$

E_0 being the nominal amplitude of the field, and ν denoting the optical frequency. $\Delta\phi$ and ΔE are instantaneous changes of the phase and amplitude caused by a spontaneous emission event. Due to the incoherence of the spontaneous emission its phase is random, which results in diffusion of the phase angle from its original value. It can be shown that the phase has a Gaussian probability distribution, and the Fourier transform of the autocorrelation of the resulting field produces a power spectrum with a Lorentzian line shape [24]. The corresponding linewidth (FWHM, Full Width at Half Maximum) is given by the modified Schawlow-Townes formula [17]

$$\Delta\nu_{ST} = \frac{\pi h \nu (\Delta\nu_c)^2}{P_i}, \tag{2.11}$$

where $\Delta\nu_c$ is the cold cavity linewidth of the laser, and P_i is the intra-cavity power of the lasing mode.

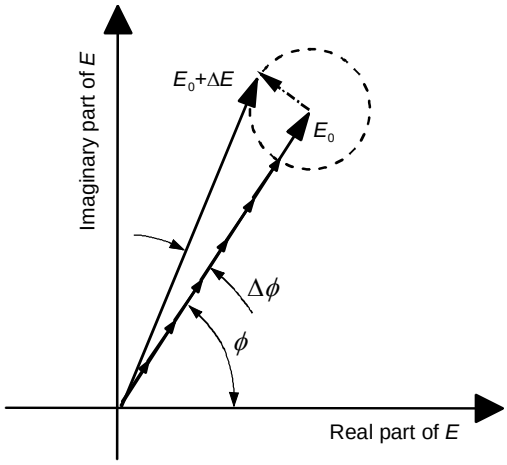

Fig. 2.2 *Instantaneous changes of phase ϕ and amplitude E_0 of the laser field due to a spontaneously emitted photon [17].*

As Eq. (2.11) indicates, linewidth is inversely proportional to the laser power. This is due to the fact that, above the laser threshold any increase in excitation leads to an increase in stimulated emission, while the spontaneous emission rate remains essentially unchanged. However, in diode lasers the lasing transition takes place between two energy bands, and the lower band is generally not empty. As a result, the laser photons can be absorbed and again re-emitted, possibly in spontaneous emission, thus leading to additional phase fluctuations. The corresponding increase in line broadening is by the spontaneous emission factor n_s, which is the ratio of the spontaneous emission rate per mode to the stimulated emission rate per laser photon.

As was already mentioned, particularly for the diode lasers the amplitude fluctuations are coupled to phase fluctuations. For this reason, any fluctuation of the field amplitude leads to additional broadening of the linewidth. This effect is taken into account by multiplying the linewidth given in Eq. (2.11) by $(1+\alpha^2)$, where α is the linewidth enhancement factor discussed in the previous paragraph. The perturbations of the field amplitude are restored to the steady-state value via damped relaxation oscillations that have a frequency typically in the order of a few gigahertz. For a free-running diode laser the relaxation oscillation frequency can be estimated from [4]

$$f_{RO} = \frac{1}{2\pi}\sqrt{\frac{G_0 S}{\tau_p}}\,, \tag{2.12}$$

where G_0 is the gain coefficient, S is the cavity photon number and τ_p is the photon lifetime (from equation 2.5). As Eq. (2.12) implies, the relaxation oscillations shift to higher frequency with increasing laser power.

After including the aforementioned effects to the modified Schawlow-Townes formula, the fundamental linewidth (ignoring the relaxation oscillation sidebands) of a diode laser is written as

$$\Delta\nu_0 = \frac{\pi h \nu (\Delta\nu_c)^2}{P_i} n_s \left(1+\alpha^2\right)\,. \tag{2.13}$$

For a multi-quantum-well InGaAlP laser diode operating around 633 nm, the typical values for both α and n_s are between 2 to 3. The cold cavity linewidth $\Delta\nu_c$ depends on

the cavity's quality factor Q, and is for a diode laser expressed as

$$\Delta\nu_c = \frac{2\pi\nu}{Q} = \frac{c}{2\pi n_d L_d}\left(\alpha_m L_d - \ln\sqrt{R_1 R_2}\right), \tag{2.14}$$

where n_d is the refractive index of the cavity medium. The quality factor of a normal solitary diode laser is relatively poor due to short cavity and low reflectance of the output mirror. The cavity quality factor can be improved, and the linewidth significantly reduced, by employing the laser diode in an external cavity (section 2.2).

The term fundamental linewidth is commonly used to refer to the power-dependent Lorentzian line arising from spontaneous emission events, and it is given by Eq. (2.13). Moreover, also power-independent spectral broadening is apparent with diode lasers, and various theories have been developed to explain this additional broadening in different cases [22,25]. At low frequencies of approximately below 1 MHz the diode laser noise is typically dominated by $1/f$ noise that provides a Gaussian contribution to the laser linewidth [22,26,27]. This type of noise is partly of intrinsic origin, but also various extrinsic reasons (so-called technical noise) broaden the diode laser linewidth. For solitary diode lasers the main elements of technical noise are current source noise and temperature noise [28]. The current source noise is due to electronic components such as operational amplifiers and voltage references of the laser current supply, and it is typically dominated by $1/f$ noise at low frequencies, and by thermal noise at higher frequencies. Also the power supply ripple is normally clearly distinguishable in the laser noise spectrum. The other important source of technical noise, temperature noise, is caused by thermal fluctuations that vary the optical length of the laser cavity. Because active temperature control is normally used, the temperature noise level is defined essentially by the quality of temperature control electronics. In external-cavity diode lasers, significant additional noise arises from mechanical vibrations and air flows that both induce fluctuations in the laser medium and cavity length. Also, temperature fluctuations are more difficult to deal with, due to the larger structural size compared to solitary diode lasers.

In practice, the laser linewidth can be determined using various techniques, most commonly heterodyne or homodyne beat frequency measurements [14]. In this work, a Fabry-Pérot interferometer was used as a frequency discriminator to study the laser frequency noise spectrum [29,30]. Although more complicated and difficult to calibrate, this method is advantageous as it provides direct information of different noise components affecting the linewidth. A typical frequency noise spectrum, i.e. the spectral density function of instantaneous frequency fluctuations, $S(f)$ [Hz/Hz$^{1/2}$], of a solitary diode laser is illustrated in Fig. 2.3.

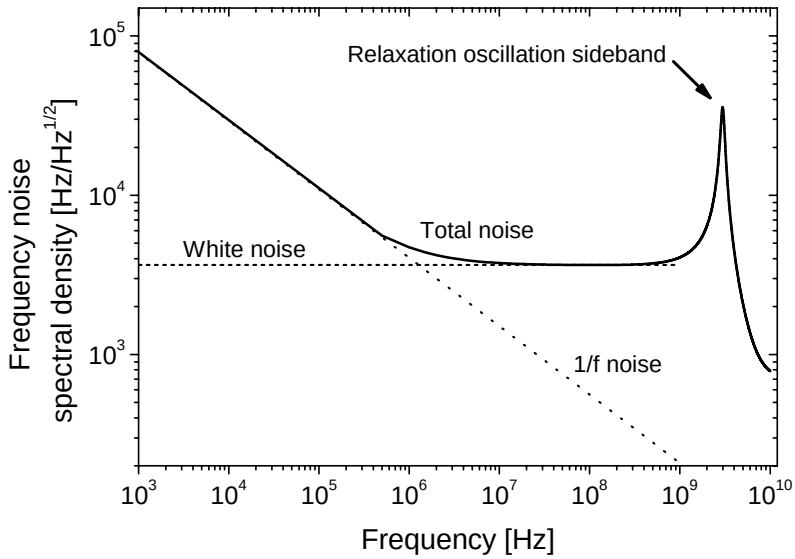

Fig. 2.3 *Typical frequency noise spectrum of a diode laser, calculated after [31]. The presented white noise level corresponds to a fundamental linewidth of approximately 40 MHz.*

2.1.4. Intensity noise

In diode lasers the main source leading to noise in optical output power is amplitude fluctuations due to spontaneous electron-hole recombination events. These events cause two types of intensity noise. First of all, they result in spontaneous emission noise, which is due to field amplitude fluctuations (Fig. 2.2). Another type of intensity noise arising from electron-hole recombination events is inversion noise, which is often referred to as shot noise. This type of noise stems from carrier number variations due to the recombination events, and it is thus affected also by nonradiative events. Although the inversion noise is a significant source of intensity noise, its effect on the diode laser linewidth is small [32].

The diode laser intensity noise can be almost shot noise limited except at frequencies close to the relaxation oscillation frequency and at frequencies smaller than approximately 1 MHz, where also other fluctuations in injection current, e.g. due to technical reasons, contribute to the intensity noise. In some cases, so-called mode partition noise may be the most severe source of intensity noise. Even if the total intensity of the laser is relatively constant, the intensity of each mode can significantly fluctuate in time. Negative correlation between the intensity fluctuations of individual longitudinal modes can lead to stabilization of the total intensity even in single-mode diode lasers, where the side modes indeed exist but are significantly suppressed relative to the main mode. Also, if the side modes are spectrally filtered, there can be a drastic increase in the total intensity noise due to the mode partition noise. On the other hand, in case of multimode lasers the negative quantum correlation between the longitudinal modes can lead to amplitude squeezing, where the total intensity noise is suppressed below the standard quantum noise limit at the expense of increased phase noise [33]. Experimental studies have shown that diode laser intensity noise can experience quite significant spatial variations within the transversal profile of the laser beam, for example due to presence of noisy nonlasing higher-order transversal modes [34].

The intensity noise is typically characterized using relative intensity noise (RIN), which is defined as a ratio of the power spectral density of the intensity noise to the square of the average optical power.

2.1.5. Spectrum and wavelength tuning

Even if single-longitudinal mode diode lasers can nowadays be fabricated, the wide and flat gain bandwidth of the diode lasers makes them inherently prone to multimode operation. A commonly used measure of the degree of single-mode operation is the side-mode suppression ratio (SMSR) which is the ratio of the main mode power to the power of the strongest side mode.

In general, a semiconductor laser oscillates at a frequency of maximum total gain [35], which is a combination of different gain components. In the case of a solitary diode laser the only components to be considered are the gain of the active material, and the resonance modes of the Fabry-Pérot cavity. The extent of semiconductor gain curve for two different lasers is demonstrated in Fig. 2.4. The frequency difference between two consecutive resonance modes, i.e. the free-spectral range (FSR) of the cavity, is given by

$$FSR = \frac{c}{2n_d L}. \tag{2.15}$$

For the 633-nm InGaAlP laser diodes used in this work L = 800 μm and the active region refractive index n_d is about 3.4. This gives an optical cavity length of 2.7 mm, corresponding to a longitudinal mode spacing of 60 GHz.

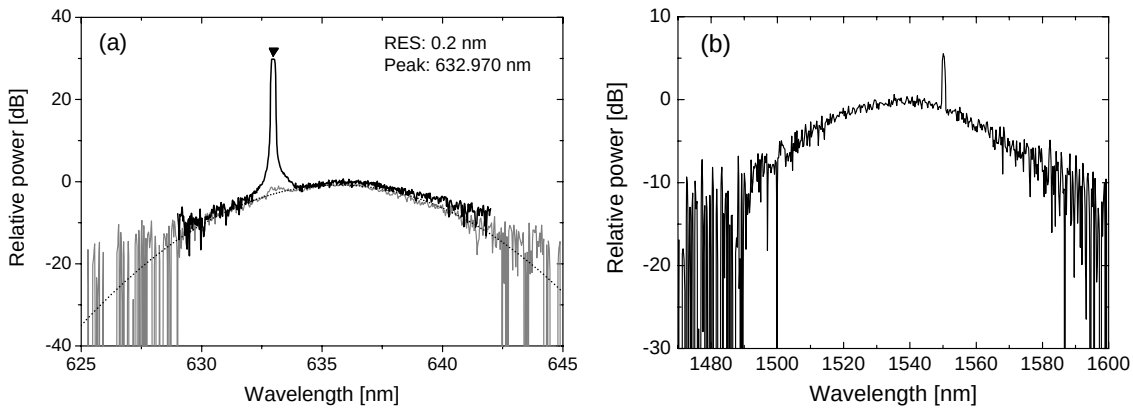

Fig. 2.4 *Measured optical spectra for two different diode lasers; (a) 633-nm InGaAlP laser, and (b) 1550-nm InGaAsP laser. Both lasers are operated in an external cavity, which explains the large difference between the lasing wavelengths and the gain curve peaks. In (a) the gray curve has been measured just below the lasing threshold (effect of the grating feedback is faintly visible at 633 nm), and the black curve shows the spectrum for a bias level of approximately 1.2 times the threshold. Curve (b) has been measured just above the threshold.*

The laser wavelength can be tuned by shifting the gain curve or the cavity resonance modes, e.g. by changing the laser diode current or temperature. The gain spectrum shifts to higher energies as the injection current increases, but as a function of temperature the change is to the opposite direction. For an InGaAlP laser diode the gain curve shifts approximately 0.23 nm/K as a function of temperature. The positions of the cavity resonance modes are altered due to the thermal expansion and due to the refractive index changes as temperature and current are varied. Within a single longitudinal mode the temperature and current dependencies are typically +0.06 nm/K (-45 GHz/K) and +0.003 nm/mA (-2.4 GHz/mA). The difference in temperature dependencies of the gain curve and resonance modes leads to mode hopping when the temperature is varied, hence limiting the attainable continuous tuning range. In addition to ambient factors,

also laser diode ageing can significantly shift the lasing wavelength. Aging drifts as large as 100 to 500 MHz per hour have been reported [36,37]. Typically the drift is largest at the beginning and at the end of the diode lifetime.

2.2. Diode lasers with optical feedback

The low quality factor of diode lasers makes them extremely sensitive to optical feedback. This sensitivity is further enhanced due to the flatness of the gain curve. The actual effect of the feedback depends on phase, magnitude, and polarization of the light fed back to the laser, and also on the feedback distance (i.e. delay time).

For various levels of optical feedback, five regimes with clearly distinguished characteristics have been experimentally identified [38] and also theoretically simulated [39]. These regimes apply to single-longitudinal mode diode lasers, although very much the same kind of behavior exists for multimode lasers as well. For very weak feedback (regime I), the laser linewidth is narrowed or broadened, depending on the phase of the feedback. When the feedback is increased, considerable line broadening occurs as a result of splitting of the emission mode, and consequent mode hopping (regime II). Further increasing feedback leads to stabilization of one of the external cavity modes, and single-mode operation with narrow linewidth is obtained for all phases of the feedback. This regime, III, covers only a small range of feedback ratio. When exceeding a certain critical value of feedback, interaction between undamped relaxation oscillations and external cavity modes leads to chaotic behavior and linewidth broadening by several orders of magnitude [35,40]. As the laser coherence length is tremendously decreased, this regime (IV) has been termed coherence collapse regime [34]. External-cavity diode lasers typically operate in the regime of strong optical feedback (V), where the laser linewidth is significantly narrowed and stable operation obtained.

Optical feedback also affects the relative intensity noise of the laser. The RIN is low for weak to moderate feedback levels (regimes I to III) but increases drastically in the coherence collapse regime. In regime V significant reduction of the RIN is observed if only single-mode operation is maintained [41,42]. In practice, a RIN level below that of a solitary diode laser can be obtained with an external-cavity diode laser. On the other hand, in an external cavity the transversal-mode control is more sensitive to adjustment of the feedback element than the longitudinal-mode control, and also the transverse distribution of the intensity noise is changed under external optical feedback.

2.2.1. Strong optical feedback

In the following, the case of strong optical feedback, which typically applies to external-cavity diode lasers, is studied in more detail in order to determine its influence on the diode laser linewidth. The effect of optical feedback can be analyzed by including feedback terms [43] in the rate equations (2.7.a)-(2.7.c). The calculation of linewidth reduction due to an external cavity usually utilizes the coupled-cavity model, which is illustrated in Fig. 2.5. For the analysis itself, various methods have been developed [43,44,45] and especially at the limit of very strong feedback ($r_3 >> r_2$) different models give different results [45]. In our case, we are no doubt operating in this regime, as the effective transmission-grating power reflectivity $R_3 = r_3^2$ is in the order of 0.08, while the AR-coated facet of the laser diode has a power reflectivity $R_2 = r_2^2$ smaller than 1×10^{-4}. Thus, in the following calculation we use the formalism described in [45], which indeed seems to give the result most consistent with our measured linewidth.

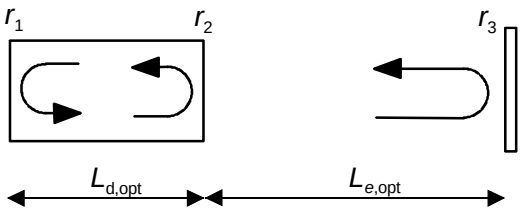

Fig. 2.5 *Model of a diode laser coupled to an external cavity. Amplitude reflectivities of the laser diode rear and output facet are given by r_1 and r_2, respectively. Similarly, r_3 is the amplitude reflectivity of the external feedback element. The round-trip times of the internal and external cavities are $t_d = 2L_{d,opt}/c$ and $t_e = 2L_{e,opt}/c$, where $L_{d,opt}$ and $L_{e,opt}$ denote the optical lengths of the cavities.*

In the case of perfect AR coating ($r_2 = 0$) the linewidth of an external-cavity diode laser can be calculated simply using Eq. (2.4), with the cold-cavity linewidth $\Delta\nu_c$ of a solitary diode laser replaced by the cold-cavity linewidth $\Delta\nu_{ecdl,c}$ of the complete external cavity:

$$\Delta\nu_{ecdl,c} = \frac{c}{2\pi\left(n_d L_d + L_{e,opt}\right)}\left(\alpha_m L_d - \ln\sqrt{R_1 R_3}\right) \tag{2.16}$$

Consequently, using equations (2.13), (2.14) and (2.16), the linewidth reduction in an ideal external-cavity diode laser can be given as

$$\frac{\Delta\nu'_{ecdl}}{\Delta\nu_0} = \left(\frac{\Delta\nu_{ecdl,c}}{\Delta\nu_c}\right)^2, \tag{2.17}$$

with $\Delta\nu_{ecdl}$' denoting the linewidth of the external-cavity diode laser and $\Delta\nu_0$ being the linewidth of the solitary diode laser.

In the coupled-cavity model, the influence of the laser diode output facet ($r_2 \neq 0$) is taken into account by the frequency dependent effective reflectivity $r_{eff}(\nu)$ of the external cavity [45]:

$$r_{eff}(\nu) = \frac{r_3 + r_2 e^{j2\pi\nu t_e}}{1 + r_2 r_3 e^{-j2\pi\nu t_e}}. \tag{2.18}$$

Above r_3 has been taken as the reference plane, and the light reflected back by r_2 has been treated as a small perturbation with a leading relative phase, as represented by the positive sign of the external cavity round-trip time $t_e = 2L_{e,opt}/c$ in the numerator.

In the case of strong optical feedback the actual lasing frequency ν is near the external-cavity resonance $\nu_{ec} = l/(t_d + t_e)$, where l is again an integer (longitudinal mode number) and $t_d = 2n_d L_d/c$ represents the round-trip time of the laser diode. The threshold condition for the laser oscillation is thus given by [46]

$$r_1 e^{(g_{th}-\alpha_m)L_d} e^{j2\pi\nu(t_d+t_e)} r_{eff}(\nu) = 1, \tag{2.19}$$

The threshold gain g_{th} and oscillation frequency ν can be obtained by writing the condition in Eq. (2.19) separately for the magnitude and argument. This provides two

coupled equations:

$$g_{th} = \alpha_m - \frac{1}{L_d}\ln\left(r_1\left|r_{eff}(\nu)\right|\right) \tag{2.20.a}$$

$$\nu - \nu_{ec} = -\frac{1}{2\pi\left(t_d + t_e\right)}\arg\left(r_{eff}(\nu)\right). \tag{2.20.b}$$

Since the real and imaginary parts of the laser diode refractive index are coupled via the linewidth enhancement factor α, the resonance frequencies ν_{ec} are not constants but depend on the threshold gain. The gain is modulated e.g. when the frequency is tuned, as the effective reflectivity $r_{eff}(\nu)$ is also varied. The dependence of the real part of the refractive index on the threshold gain is approximately [46]

$$n_d = n_{d0} + \frac{\alpha c}{4\pi\nu}\left(g_{th} - g_{th0}\right), \tag{2.21}$$

where n_{d0} is the refractive index and $g_{th0} = \alpha_m - \ln(r_1 r_2)/L_d$ the threshold gain of the solitary diode laser. Combining this gain dependent refractive index with Eq. (2.20.a) and (2.20.b) gives

$$\nu_{ec} = \nu + \frac{\alpha\ln\left(\left|r_{eff}(\nu)\right|/r_3\right) - \arg\left(r_{eff}(\nu)\right)}{2\pi\left(t_{d0} + t_e\right)}, \tag{2.22}$$

where t_{d0} is the round-trip time of the solitary diode laser without external feedback.

Now, the actual linewidth $\Delta\nu_{ecdl}(\nu)$ of the external-cavity diode is frequency dependent and can be calculated from Eq. (2.22) using the transmission-line model [43]. Under very strong optical feedback the linewidth is given by [45]

$$\Delta\nu_{ecdl}(\nu) = \Delta\nu'_{ecdl}\left(\frac{d\nu_{ec}}{d\nu}\right)^{-2}. \tag{2.23}$$

As could be expected, at the limit of residual reflectivity r_2 approaching to zero, the laser linewidth calculated using Eq. (2.23) is equal to $\Delta\nu'_{ecdl}$ predicted by Eq. (2.17).

As an example, curve (a) in Fig. 2.6 shows the calculated linewidth for the 633-nm transmission-grating laser of this work [Publ. II], when the laser is detuned by sweeping the cavity length. In this particular case the external cavity provides linewidth reduction by a factor of ~ 1500. The influence of the non-ideal AR coating of the laser diode facet is seen as a small modulation that has period $1/t_e$. The same periodical variation is evident also in the threshold gain of the laser, which can be calculated using Eq. (2.20.a).

To demonstrate the importance of good-quality AR coating, curve (b) of Fig. 2.6 shows the linewidth calculation also for a higher value of the diode output facet reflectivity. In this case the linewidth is strongly dependent on the cavity detuning, and also the asymmetry [46] as a function of detuning due to the linewidth enhancement factor α is clear.

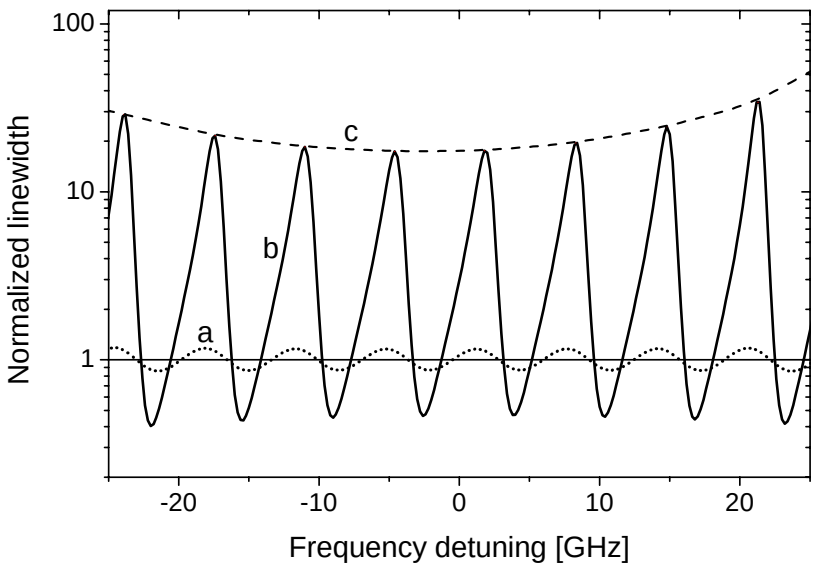

Fig. 2.6 *Theoretical variation of the transmission-grating laser linewidth as a function of frequency detuning. The linewidth is given normalized to that (35 kHz) of the ideal (r_2 = 0) external-cavity laser. Laser wavelength is 633 nm, the output power is 8 mW, the linewidth enhancement factor $\alpha = 2.5$, and the grating reflectivity (including the feedback coupling efficiency) is assumed to be 8%. Optical length of the external cavity is 23 mm. Laser diode output facet reflectivity is 8×10^{-5} for curve (a) and 8×10^{-3} for curve (b). Envelope curve (c) shows the effect of the grating dispersion, which has a Gaussian shape.*

In summary, the preceding analysis shows that using a laser diode with good AR coating in an external cavity allows one to obtain narrow linewidth that is virtually independent of the lasing frequency. This is not the case for higher values of the diode output facet reflectivity, due to the already mentioned fact that the linewidth enhancement factor makes the oscillation frequency ν_{ec} dependent on the laser threshold gain. For the same reason, at higher values of r_2 (or smaller levels of external feedback r_3), the competition between the coupled cavities can create bistable frequency zones with multiple thresholds. The stable operation range is given by the condition $d\nu_{ec}/d\nu > 0$, which can be obtained by performing stability analysis of the characteristic matrix that describes the laser under optical feedback [43].

Considering spectroscopic applications, especially beneficial effect of the AR coating is the increase in mode-hop-free tuning range of the external-cavity laser. Typically, the AR-coated surface has to have a residual reflectivity smaller than ~ 0.1% in order to remarkably improve the continuous tuning range [47,48]. Coating also provides a nearly constant tuning slope, i.e. the laser frequency changes approximately linearly with the cavity length. This is important especially in applications where frequency modulation is used, since a nonlinear tuning slope produces modulation distortion. In practice, the ECDL cavity also contains a collimating lens, which is needed to fulfill the stability condition of the resonator. Naturally, the collimating lens (and possible other optics inside the cavity) must be AR-coated in order to minimize the coupled-cavity effects.

2.3. Diode lasers with optical injection

Figure 1 shows schematically the principle of diode laser injection locking. Light from the master laser is injected into the slave laser through an optical isolator that blocks the reverse light path. Also this system can be analyzed using the rate equations for a single-mode diode laser. Adding the injection terms to the equations (2.7.a)-(2.7.c) gives the following rate equations for an injection-locked diode laser [49,50]

$$\frac{dS(t)}{dt} = \left[G_0\left(N(t) - N_{th}\right) + 2FSR\sqrt{\frac{S_{inj}(t)}{S(t)}}\cos\left(\phi_{inj}(t) - \phi(t)\right)\right] S(t) \tag{2.24.a}$$

$$\frac{d\phi(t)}{dt} = \frac{\alpha}{2} G_0\left(N(t) - N_{th}\right) - 2\pi\Delta f + FSR\sqrt{\frac{S_{inj}(t)}{S(t)}}\sin\left(\phi_{inj}(t) - \phi(t)\right) \tag{2.24.b}$$

$$\frac{dN(t)}{dt} = \frac{I(t)}{e} - \frac{N(t)}{\tau_N} - G_0\left(N(t) - N_{tr}\right). \tag{2.24.c}$$

The frequency detuning between the master and slave lasers is defined as $\Delta f = \nu_{\mathrm{inj}} - \nu_{\mathrm{s}}$, where ν_{inj} denotes the master frequency and ν_{s} is the unperturbed cavity frequency of the slave laser. The phase of the injected field is $\phi_{\mathrm{inj}}(t)$, and the number of injected photons inside the slave laser cavity is $S_{\mathrm{inj}}(t)$. Other parameters were defined previously in section 2.1.1 and now refer to the slave laser.

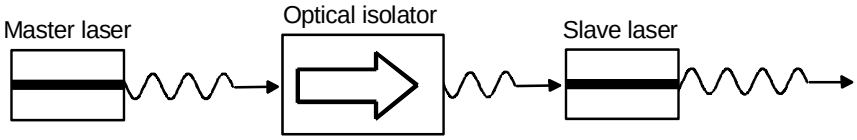

Fig. 2.7 *Schematic of the master-slave laser system. Light from the master laser is injected into the active region of the slave laser. Optical isolator is used to ensure unidirectional coupling.*

All the parameters in the set of equations (2.24) are given inside the slave laser cavity. However, there must be some way to connect the master laser field outside of the slave laser cavity with the field injected inside the slave laser cavity. In practice this coupling depends on the output facet reflectivity of the slave laser, but also e.g. on the spatial mode matching between the master and slave fields. Because the coupling can be quite complicated to analyze, we restrict to study the photon number inside the slave laser cavity without any attempt to define theoretical coupling efficiency. Instead, to allow comparison between the theoretical and experimental results, the injection coupling efficiency is estimated experimentally for each measurement. The used method is explained in Publications III and IV.

Again, the static state of the slave laser can be solved by setting the time derivatives in Eqs. (2.24.a)-(2.24.c) to zero. This leads to two important results. First, the injected field increases the stimulated emission and thus reduces the carrier density compared to the threshold value N_{th} of the free running slave laser. This in turn leads to reduced gain. Secondly, it can be shown that the slave laser can lock to the frequency of the master laser only within a certain master-slave frequency detuning Δf, and this static locking range is given by [50,51]

$$-\frac{FSR}{2\pi}\sqrt{\frac{S_{inj}}{S}}\sqrt{1+\alpha^2} < \Delta f < \frac{FSR}{2\pi}\sqrt{\frac{S_{inj}}{S}} \,. \tag{2.25}$$

It is clear from Eq. (2.25) that the locking range is increased with the injection ratio S_{inj}/S. The locking range is also proportional to the slave laser free-spectral range, *FSR*. This can be understood so that the injected field adds to the field propagating inside the slave laser cavity at a time interval $1/FSR$, which is the cavity round-trip time [52].

In practice, the locking properties depend on the total gain profile of the slave laser and locking can be obtained by injecting light at a frequency which is close to a side mode instead of the free-running mode of the slave laser (Fig. 2.8). Also in this case the shape of the locking band follows the condition (2.25), although the locking range may be decreased or enhanced compared to the intra-mode locking, depending on the mode number [53].

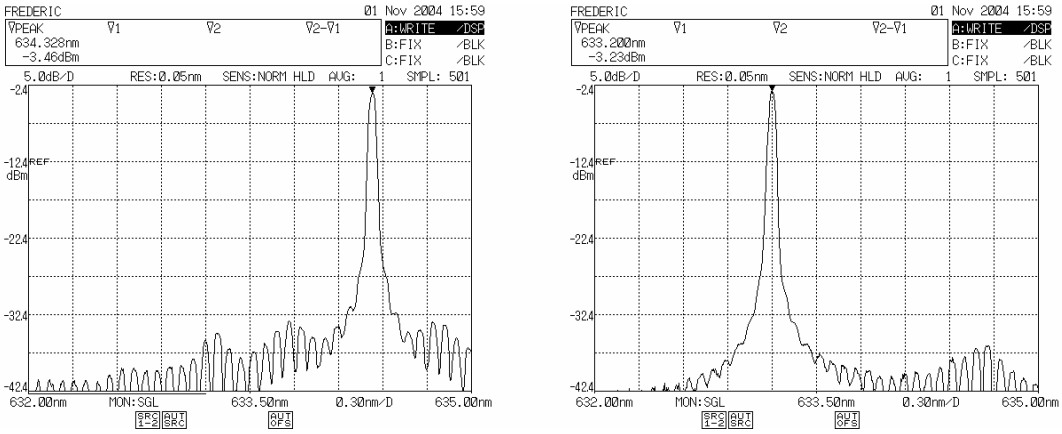

Fig. 2.8 *(left) Measured spectrum of a microlens-coupled diode laser when running freely, and (right) when injected with light from an external-cavity laser. Injected wavelength is close to the second side mode of the microlens cavity at the short-wavelength side of the free-running mode. Smaller structure in the spectra is due to the diode laser cavity, which has an optical length of ~ 2.7 mm.*

Due to the phase-gain coupling described by the linewidth enhancement factor α the locking range is asymmetric. This asymmetry has been explained by Lang [52] as follows: The decrease in carrier number due to the light injection results to increased refractive index and subsequently to decreased cavity resonance frequency of the slave laser. Therefore, the optimum locking can be obtained when the injected frequency coincides with the cavity resonance frequency that is downshifted compared to the cavity resonance of the free-running slave laser.

It is important to notice that injection locking is not necessarily stable within the whole locking range given by Eq. (2.25) but there are also dynamically unstable regions [51,52]. The dynamical instabilities are not necessarily detrimental in all applications, since they are typically observed as additional spectral components a few gigahertz apart from the component locked to the frequency of the master laser. However, in most applications, such as in optical communications the dynamical instabilities must be considered. Just like in the case of a diode laser subjected to optical feedback, the system described by the set of rate equations (2.24) can be checked for dynamical stability by examining the eigenvalues of the characteristic matrix of the system [43,51]. This is discussed in more detail in section 4.2, in which the modulation transfer

properties of injection-locked diode lasers are analyzed. An example of experimentally observed instabilities is given in Fig. 2.9.

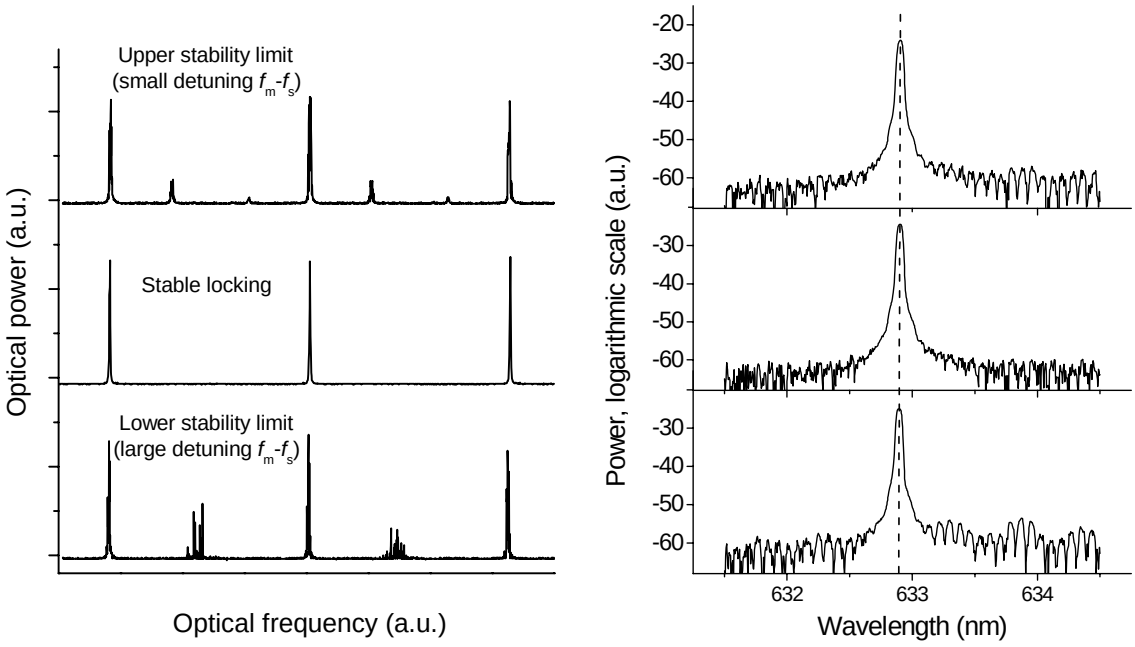

Fig. 2.9 *Optical spectra for different values of master-slave detuning. (Left) Measured with a Fabry-Pérot (FP) interferometer. The separation of the large peaks corresponds to the free spectral range (2 GHz) of the FP-interferometer, i.e. the laser spectrum is repeated after every 2 GHz. (Right) The respective spectra measured with a diffraction-grating spectrum analyzer.*

Usual dependence of the static and dynamic locking ranges on the injection ratio is sketched in Fig. 2.10. For large values of the linewidth enhancement factor α, damping is reduced and the dynamically stable region is narrowed compared to a diode laser with small α, even if the static locking range is broadened with α. Relatively good agreement between the experimental and theoretical locking ranges has been reported [51,54].

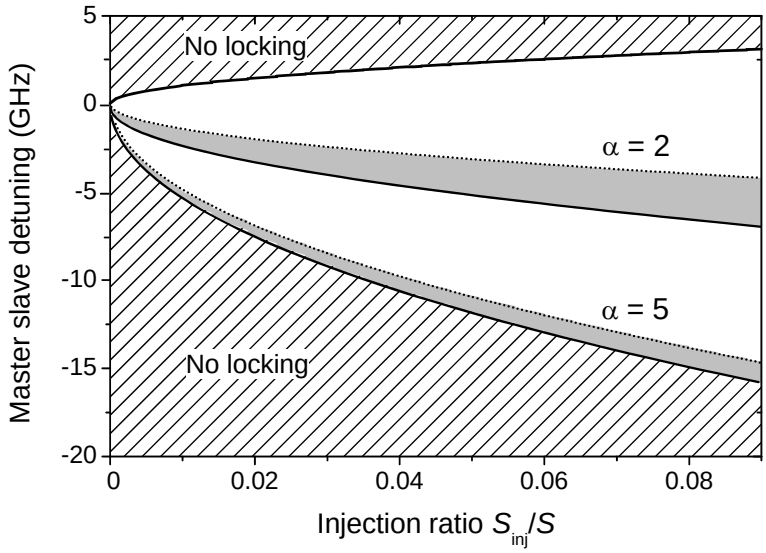

Fig. 2.10 Theoretical estimate [50] of the injection-locking range for two different values of linewidth enhancement factor α. Solid lines give the boundaries of the static locking range, and the filled areas denote the dynamically stable regions. At very low and high values of injection ratio stability may be obtained over the entire locking range (not shown in the figure).

In practice, the picture of slave laser output state for different ratios of optical injection and master-slave detuning is not as simplified as depicted in Fig. 2.10. Instead, various regions with clearly distinct characteristics have been found both within and outside of the static locking range [55,56,57]. Due to the complex nature of injection locking, simple classification similar to that for the optical feedback regions is difficult to make, and the locking characteristics of different diode lasers can be very different. The situation is further complicated e.g. in the presence of external optical feedback, which competes with the injection and hence reduces the attainable locking range. This effect can be analyzed by including both the feedback and injection terms in the rate equations [8]. A good overview on the general properties of diode laser injection locking is given in Ref. [3].

2.4. Doppler-free spectroscopy of molecular iodine

For applications where the means of passive stabilization do not provide sufficient frequency stability, the laser can be actively stabilized on a more stable reference. In order to obtain absolute and precise long-term stabilization, atomic and molecular absorption lines are commonly used. A good frequency reference should be reproducible and thus virtually independent of external perturbations, such as temperature and pressure variations, or electric and magnetic fields. For that reason, molecules with no permanent dipole moment, such as the iodine (I_2) molecule, are the most suitable ones. Iodine has approximately 100 000 absorption lines in the visible, making it one of the most important references for laser stabilization. The absorption lines are limited by Doppler broadening to a width of ~ 1 GHz, but much narrower linewidths can be observed using nonlinear spectroscopic techniques to resolve their hyperfine structures [19].

As a part of this work, a laser spectrometer was designed and constructed. The spectrometer utilizes saturation spectroscopy in an external absorption cell for resolving the Doppler-free spectrum of iodine. Wavelength modulation technique is used to lock the laser frequency to an iodine hyperfine component. The actual setup is described later in chapter 4, here only the fundamentals of iodine as a molecular reference and the principle of the used spectroscopy technique are discussed.

2.4.1. Iodine as a frequency reference

The rich absorption spectrum of iodine results from a combination of three contributions: electronic energy due to the motion of electrons about the nuclei, vibration of the nuclei, and rotation of the molecule about its center of gravity. In each electronic state the molecule has a number of possible vibrational energy levels, and in each of these, a number of rotational energy levels. In Fig. 2.11, the lowest energy states of iodine are schematically shown, together with some of the vibrational substates.

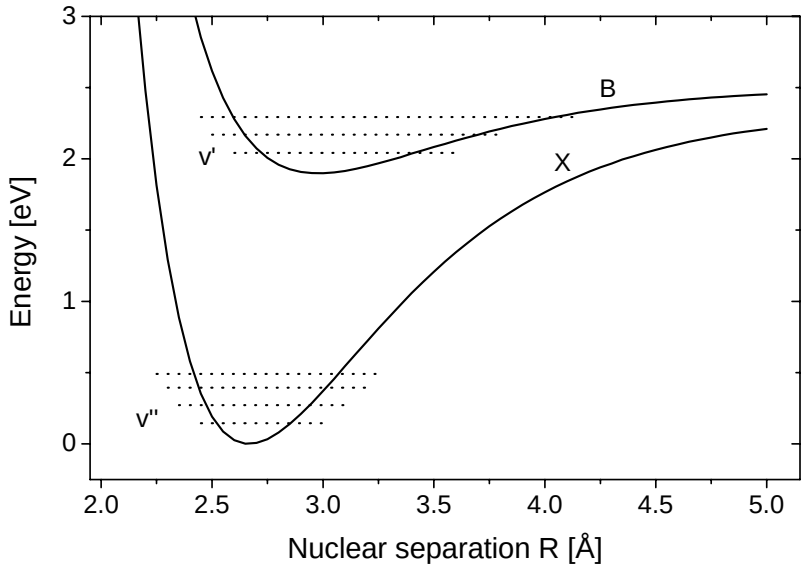

Fig. 2.11 *Ground state (X) and excited state (B) of the I_2 molecule, together with some of the corresponding vibrational substates (v´´ and v', respectively).*

As a transition between electronic states occurs, also the vibrational and rotational states can change. However, not all transitions are allowed. For the rotational quantum number J the selection rule is $\Delta J = J' - J'' = \pm 1$. Thus, the allowed transitions consist of two sets of lines: those with lower frequencies are referred to as P branch ($\Delta J = -1$), and those with higher frequencies are referred to as R branch ($\Delta J = +1$). For the vibrational quantum numbers there is no selection rule if the transition occurs between two electronic states. However, the transition probabilities are proportional to so-called Franck-Condon factors that describe the overlap of two vibrational wave functions. According to the Frank-Condon principle, the transitions take place instantly, so that the nuclear separation does not change. That is to say, the transitions vertically upward or downward in the potential energy diagram correspond to the most intense lines.

The transitions in the B-X system of I_2 are commonly identified by denoting first the change of rotational quantum number (P- or R-branch) and after that, in parenthesis, the rotational quantum number of the ground state. The vibrational quantum numbers of upper and lower state are given both, respectively. For example, the line R(127)11-5 used in He-Ne laser stabilization corresponds to a transition from J' = 128, v' = 11 of the upper electronic state to J'' = 127, v'' = 5 of the ground state.

Coupling between the total molecular angular momentum and total nuclear angular momentum leads to further energy splitting and hyperfine structure of the absorption lines [58,59]. The number of main hyperfine components is 15 for even rotational quantum number J'', and 21 for odd J''.

2.4.2. Line broadening and saturation spectroscopy

In iodine, two types of mechanisms cause absorption line broadening: homogeneous broadening affects each molecule identically, while inhomogeneous broadening distributes the resonance frequencies of molecules over some spectral range.

Inevitable natural broadening originating from spontaneous emission sets the lower limit for the transition linewidth. In red, the natural linewidths of the iodine hyperfine components are of megahertz order, but at shorter wavelengths much narrower lines

exist – for example, natural linewidths as narrow as ~ 40 kHz have been found at 508 nm [60]. Another homogeneous broadening mechanism having a significant effect is pressure broadening, which is due to the collisions of molecules. In experiments around 633 nm the iodine pressure is typically set to 17.3 Pa, resulting to a homogeneously broadened linewidth of approximately 3 MHz [61]. It should be noted that in practice the observable line is the convolution of the hyperfine component with the laser line. However, in our case the laser line is so narrow that its influence is fairly small (section 3.2). Instrumentation-related broadening also includes e.g. the transit-time broadening and saturation (or power) broadening effects. In the experimental setup described in section 4.1 relatively small beam intensity is used and hence the effect of saturation broadening is also quite small, approximately 200 kHz (FWHM). The transit-time broadening can be estimated [19] to be of the order of 100 kHz (FWHM) for the experimental conditions, with the laser beam diameter being approximately 2 mm.

The inhomogeneous broadening arises mostly from the thermal motion of the molecules. The transition frequencies of the molecules are Doppler shifted when they are moving relative to the observer, and thus this type of broadening is called Doppler broadening. Due to this effect, linewidths of the I_2 hyperfine components are increased up to ~ 360 MHz at room temperature [62].

The intensity profile of a homogeneously broadened line is Lorentzian, while the Doppler broadening leads to a Gaussian profile. The overall lineshape of a transition is the convolution of these profiles, and it has a Voigt profile [19]. However, in the case of iodine absorption, the Doppler broadening is predominant and the Gaussian profile may be used as a good approximation of the Voigt profile. The narrow Lorentzian hyperfine components can be resolved from the Gaussian background e.g. by using velocity-selective saturation of the Doppler-broadened transitions. This technique, referred to as saturation spectroscopy, is discussed next.

Let us first consider absorption in case of a homogeneously broadened line. If the beam intensity I_0 is relatively weak, so that it does not significantly change the state of the medium, the absorption is linear and is given simply by the Lambert-Beer law [19]

$$I(z) = I_0 e^{-\sigma(N_{I1}-N_{I2})z} = I_0 e^{-\sigma \Delta N_{I0} z} = I_0 e^{-\alpha_0 z}, \tag{2.26}$$

where σ is the absorption cross section of the transition, z is the beam path length in the absorbing medium, and α_0 is (unsaturated) absorption coefficient. N_{I1} and N_{I2} are the populations of the lower and upper energy states, which are assumed to be nondegenerate. (Naturally, the absorption is also a function of frequency although not explicitly indicated in Eq. (2.26)).

In thermal equilibrium relation $N_{I1} >> N_{I2}$ holds, but as the beam intensity I_0 is increased the two populations start to equalize, i.e. the absorption starts to saturate. In this case, the absorption coefficient is given by [63]

$$\alpha_S = \frac{\alpha_0}{1 + (I_0/I_S)}. \tag{2.27}$$

In Eq. (2.27) I_S denotes the saturation intensity, which is defined as the intensity required to obtain a population difference that is half of its thermal equilibrium value. (I.e. for $I_0 = I_S$ we get $\Delta N_I = ½\, \Delta N_{I0}$ and thus $\alpha_S = \alpha_0/2$). As an example, the saturation intensity for the transition R(127) of $^{127}I_2$ is shown as a function of pressure in Fig. 2.12. In this work, iodine pressure of 17.3 Pa has been used, corresponding to a saturation intensity of approximately 22 mW/mm^2.

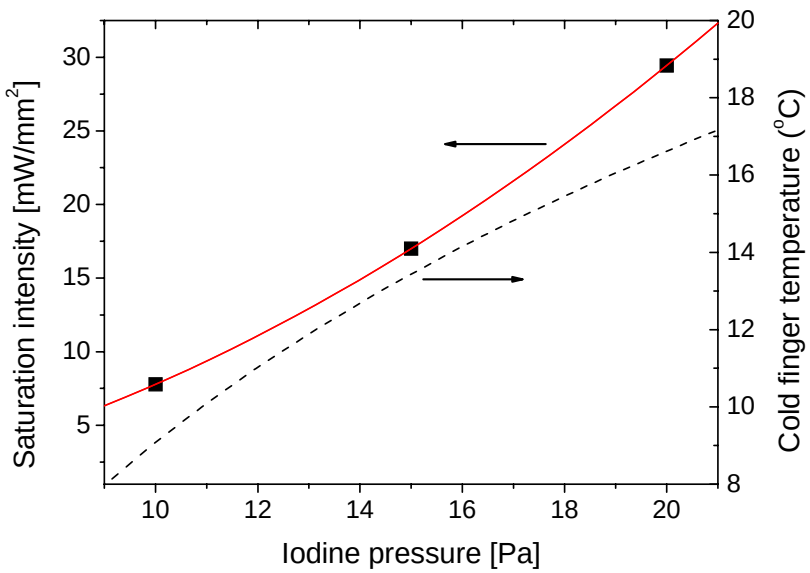

Fig. 2.12 *Saturation intensity as a function of iodine pressure for the transition R(127). The solid curve is a second order polynomial fit to the three data points obtained from Ref. [61]. Dashed curve shows the corresponding cold finger temperature of the iodine cell. (Note the unit of the saturation intensity – used for practical convenience).*

Let us now consider an iodine hyperfine line that is inhomogeneously broadened. When using a narrow-linewidth laser, it affects only the molecules that have a certain velocity component in the beam direction. If the beam is first passed through an absorption cell and then reflected back to the cell according to Fig. 2.13, the two beams – referred to as pump and probe beam – are counterpropagating and thus affecting the molecules with opposite Doppler shifts (Fig. 2.14 a). Now, if the laser frequency is tuned to coincide with the center of the transition, both beams interact with the same molecules, i.e. those with zero velocity in the beam direction. This way the hole burned by the pump beam into the inhomogeneous line can be detected as an increase in the probe beam intensity. The corresponding dip at the center of the absorption profile is called the Lamb dip (Fig. 2.14 b). If the laser linewidth is narrow enough to be ignored, the depth of the Lamb dip depends on the properties of the absorbing medium, as well as on the intensities of the pump and probe beams [19].

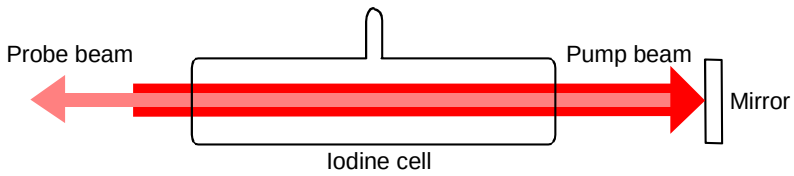

Fig. 2.13 *In the saturation absorption experiment of this work the pump beam is reflected back as a probe beam.*

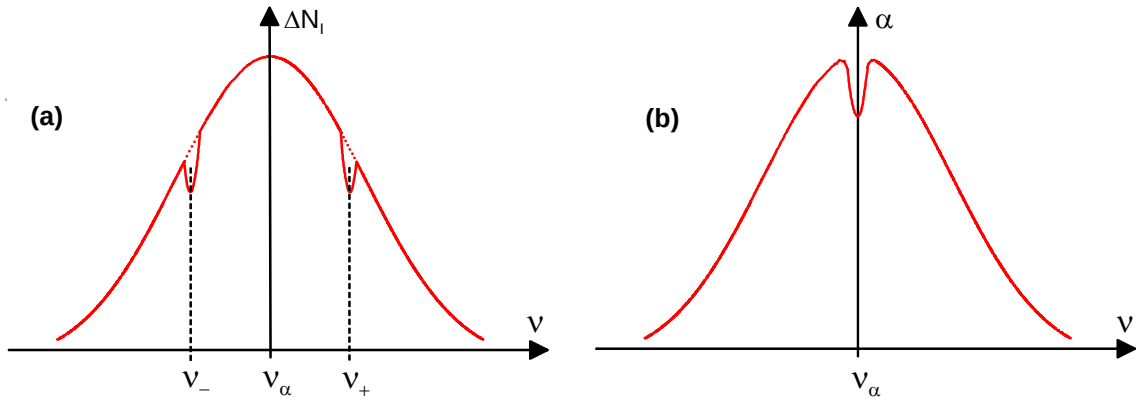

Fig. 2.14 *(a) The population difference ΔN_I of the upper and lower states as a function of optical frequency ν. So-called Bennet holes burned at sides of the curve correspond to the Doppler-shifted frequencies $\nu_- = \nu_\alpha(1-v/c)$ and $\nu_+ = \nu_\alpha(1+v/c)$, where ν_α is the center absorption frequency and $\pm v$ is a velocity component of the group of molecules excited. Fig. (b) shows the Lamb dip at the center of the absorption profile when both the pump and probe beams interact with the same molecules ($v = 0$).*

Typically, the hyperfine components are so weak that detection of their inverse Lamb dips with a direct intensity measurement is very difficult. In this work, the (standard) third-harmonic technique [64] is used to improve the signal-to-noise ratio of the detection and to lock the laser frequency to a hyperfine component. The third-harmonic technique is a version of wavelength modulation (WM) spectroscopy, in which the laser frequency is modulated with a sinusoidal signal at a frequency smaller than the absorption linewidth. The nonlinear absorption profile leads to a generation of amplitude modulation with signals at different harmonics of the modulation frequency. The approximative *n*th derivative of the absorption profile can be measured by detecting the *n*th harmonic component of the modulation frequency in the probe beam intensity with a lock-in amplifier [19]. In order to get a dispersive error signal suitable for frequency locking an odd derivative must be used.

The improved signal-to-noise ratio obtained with the *n*th harmonic technique is due to two reasons: First of all, the detection is restricted to a narrow frequency interval centered at the demodulation frequency. Secondly, the $1/f$ noise is reduced as the detection is shifted from DC to higher frequencies. The importance of the good signal-to-noise ratio (SNR) becomes evident from the formula that gives the frequency stability slope, or Allan deviation [65], attainable with a frequency reference:

$$\sigma_y(2,\tau) = \frac{\Delta\nu_\alpha}{\nu_\alpha}\frac{1}{\mathrm{SNR}}\frac{1}{\sqrt{\tau}}. \tag{2.28}$$

In Eq. (2.28) $\Delta\nu_\alpha$ is the FWHM of the transition, ν_α its center frequency, and τ the integration time. Note that the frequency stability is proportional also to the transition linewidth, which justifies the use of the narrow hyperfine components.

In general, the signal-to-noise ratio declines rapidly when using higher harmonic frequencies because the signal amplitude is getting smaller. On the other hand, at higher harmonics the effects of the Doppler-background and the frequency shift caused by asymmetry of the absorption line profile are reduced [66]. To summarize, the third-harmonic technique is commonly used as it leads to better accuracy than use of the first harmonic, and yet gives reasonably good signal-to-noise ratio.

2.4.3. Frequency shifts in iodine

The frequency reproducibility and the determination accuracy of the absorption line center are affected by various frequency shifts arising from fundamental and technical reasons. In many of the present-day frequency stabilization setups that have been carefully realized, the major contribution shifting the centers of the transitions comes from iodine impurities [67]. However, also other significant effects should be taken into account.

One of such frequency shifts in iodine is pressure shift, which is due to elastic collisions of the molecules inside the absorption cell [19]. The shift is linear and at the 633 nm wavelength and ~ 17 Pa pressure its magnitude has been measured to be smaller than -10 kHz/Pa [68,69]. In order to minimize the effect of the pressure shift, the temperature of the cell's coldest spot (cold finger) has to be carefully controlled, since it determines the iodine pressure. Around 17.3 Pa the dependence of the iodine pressure on the cold finger temperature is approximately 0.66 Pa/°C (Fig. 2.12), which means that the frequency shift as a function of temperature is smaller than -15 kHz/°C.

Another important frequency shift is power shift, which can be quite different for different setup configurations. For configurations similar to the one used in this work, the effect of saturation power on the line frequency has been found to be almost negligible at small intensities [67,68]. However, when the one-way saturating intensity exceeds the value ~ 5 mW/mm^2, power shift becomes of importance, being of the order -4.3 kHz/mW. (Measured in a configuration where the pump beam is reflected back as a probe beam [68]). This suggests that, for good reproducibility, the average saturating intensity should be kept relatively low even if the signal-to-noise ratio and thus the laser stability are degraded. Also, the alignment of the pump and probe beams is critical, since even a small misalignment reduces the signal amplitude and affects the reproducibility [67].

In general, frequency dependence on the operation parameters is due to the asymmetry in the observed line profile of the hyperfine components [62]. A typical shift related to the line asymmetry is modulation amplitude shift, which is approximately -10 kHz/MHz [68]. (When using 3rd harmonic technique, the modulation amplitude that gives the best SNR is approximately three times the effective linewidth under study [70], i.e. ~ 10 MHz in case of the iodine hyperfine components). The asymmetry has been ascribed e.g. to a frequency dependent self-action of light in the iodine cell associated to the beam geometry [62], wave front curvature [71], collisions of iodine molecules [61], and frequency pushing and pulling of the neighboring lines [59,66]. Frequency shifts can be minimized for instance by using a laser beam with high spatial quality, by using sufficiently small modulation amplitude, and by avoiding optical feedback, which is a source of modulation distortion [72]. Also, when using WM spectroscopy, spurious intensity modulation should be minimized. Spurious intensity modulation is generated e.g. due to etalon effects but also when modulating the diode laser frequency. In section 4.2 use of laser injection locking has been studied as a conceivable method for reducing the spurious intensity modulation.

3. EXTERNAL-CAVITY DIODE LASERS

Various technologies have been developed for reducing diode laser linewidth and for facilitating their wavelength tuning. In the infrared, one of the latest and most important inventions are the quantum cascade lasers [73], which are used e.g. in trace gas analysis [74]. In the near infrared and especially in telecommunication applications devices with integrated optical feedback elements, such as DBR (Distributed Bragg Reflector) and DFB (Distributed Feedback) lasers, [21] are commonly used. In visible wavelengths such devices do not exist or the availability is limited. Therefore, the most common solution is to operate the diode laser in an external cavity. The external-cavity diode lasers (ECDL) still find use also in wavelength regions where integrated devices are available. For instance, in test and measurement equipment ECDLs are used due to their typically narrow linewidth and good tunability compared to the DBR and DFB lasers.

Also the variety of different ECDL designs is huge as they have been used and designed for several different applications. Most of the designs are based on one of the two basic configurations, the Littrow configuration or the Littman-Metcalf configuration (Fig. 3.1). The Littrow structure is simple and thus easier to stabilize, but it has a problem of varying output beam pointing associated with laser wavelength tuning which is made by rotating the grating. The Littman-Metcalf configuration removes this problem, although at the expense of increased complexity. Despite the fact that ECDLs have been extensively developed and used in research laboratories and in commercial applications already for more than two decades, many new implementations have been reported also lately [75,76,77,78]. One of the quite recent designs is the transmission-grating diode laser developed previously at MRI* [9], and also used in this thesis.

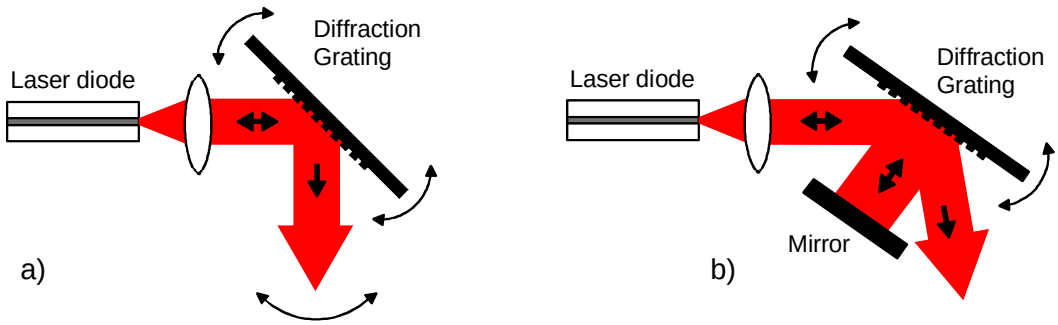

Fig. 3.1 *External-cavity diode laser (a) in basic Littrow configuration and (b) in Littman-Metcalf configuration.*

The principle of the transmission-grating diode laser is shown in Fig. 3.2. The -1 order reflection from the grating is used for optical feedback, while the laser output beam is obtained as the zeroth order transmitted beam trough the grating. The transmission gratings are manufactured onto a SiO_2 substrate and the other side of the substrate is typically antireflection coated. The details of the design and manufacturing are given in Ref. [9]. Similarly to the ECDLs in general, the laser frequency can be tuned by rotating the grating and/or by tuning the laser cavity length. In order to achieve large mode-hop free tuning range, the grating angle and the laser cavity length must be synchronously varied so that the grating dispersion curve follows the lasing mode of the cavity.

* Metrology Research Institute, Finland

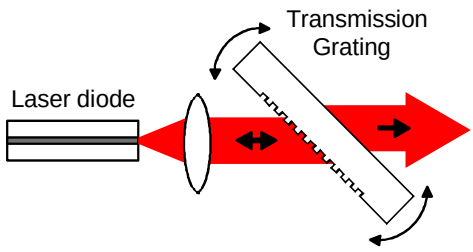

Fig.3.2 *Transmission-grating version of the Littrow-configuration.*

The main advantage of the transmission-grating geometry is that it removes the problem of varying output beam pointing, while still allowing the use of the simple Littrow-configuration. The invariant beam pointing is useful e.g. when coupling laser output light into an optical fiber, and crucial in saturation spectroscopy and injection-locking experiments, where already a minor change in the beam alignment can spoil the system performance. The simple Littrow-structure is possible to make compact, extremely robust, and symmetrical relative to the optical axis. The resulting high mechanical stability of such transmission-grating laser provides enhanced frequency reproducibility and ensures inherently narrow technical linewidth. In this work, two different transmission-grating lasers were constructed – one for the 1.55-µm optical telecommunication band, and the other one for spectroscopy applications in the 633-nm wavelength band.

3.1. 1550-nm transmission-grating diode laser

Publication I reports the structure and characteristics of the constructed 1.55-µm band laser. The mechanical construction is similar to that depicted in Ref. [9]. The used laser source is an AR-coated InGaAsP diode laser (Sacher Lasertechnik GmbH SAL-1550-05), which has a residual reflectivity of the output facet of smaller than 1.3×10^{-5}.

The primary aim was to demonstrate operation of the transmission grating in the telecommunication wavelengths, where the need for tunable narrow-linewidth sources is pronounced, and where the gain bandwidths of the laser diodes are typically much larger than with the visible-wavelength devices. Reliable single-mode operation (Fig. 3.3) of the 1.55-µm transmission-grating was indeed demonstrated over the whole gain band of the laser diode. The wavelength tuning range (without temperature tuning) is 128 nm and covers the entire S- and C-bands of optical telecommunications (Fig. 3.4). The coarse tuning can be reached by tilting the grating angle manually with fine adjustment screws. The continuous fine-tuning range of the laser frequency was demonstrated to be 30 GHz, which is limited by the maximum expansion of the PZT elements used for tuning.

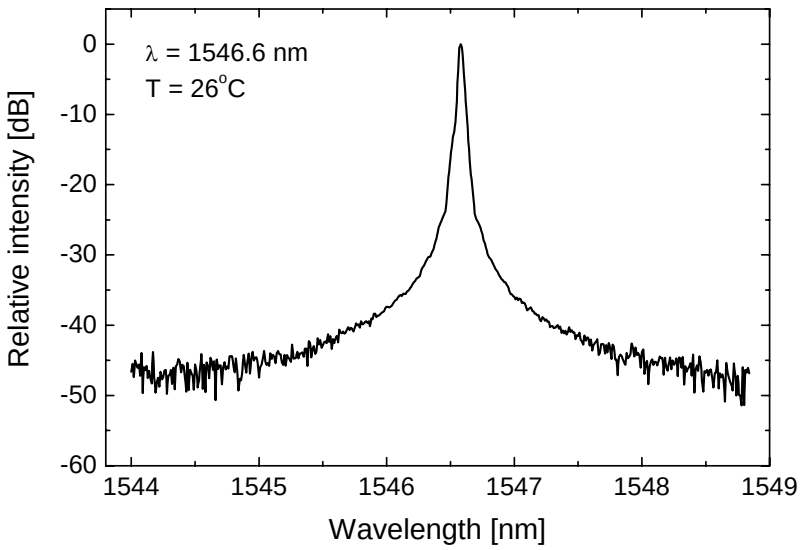

Fig.3.3 *Measured spectrum of the 1.55-μm transmission-grating laser. Close to the gain curve maximum (Fig. 2.4 b) SMSR better than 40 dB is obtained. At the positive-wavelength side the SMSR is typically better than 30 dB and at the negative-wavelength side smaller than that.*

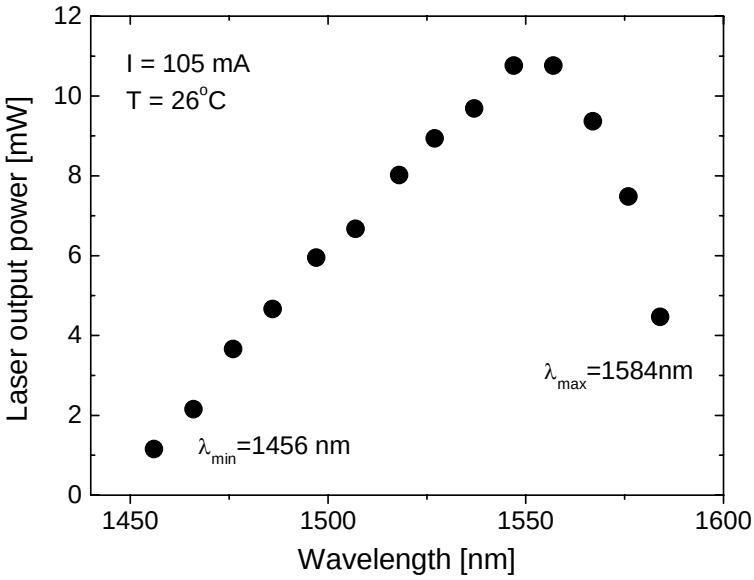

Fig. 3.4 *Output power of the 1.55-μm transmission-grating laser as a function of wavelength tuning.*

In Publication I, also the transmission grating operation with different polarizations, transverse electric (TE) and transverse magnetic (TM) polarization has been studied. It was observed that the grating works very well in TM polarization but in TE polarization the measured characteristics strongly differ from the calculated ones. Further calculations indicated that TE polarization is in general more sensitive to variations of the grating parameters and the difference between the designed and measured values can be explained e.g. by fabrication errors. In practice, optimal laser operation was reached in TM polarization. For instance, for TM polarization the grating feedback was observed to be almost constant as a function of wavelength, while with TE polarization the diffraction efficiency changes with wavelength.

3.2. 633-nm transmission-grating diode laser

The 633-nm transmission-grating laser reported in Publication II is intended particularly for accurate absolute frequency measurements of narrow (FWHM ~3 MHz) hyperfine components of iodine. In such measurements, the laser is conventionally locked to a hyperfine component and the laser frequency is subsequently measured. For steady frequency locking, the laser is required to have intrinsically good passive frequency stability. Also, the laser linewidth should be sufficiently narrow, preferably smaller than that of the hyperfine components. Even though ECDLs have greatly improved spectral purity compared to solitary diode lasers, their frequency is very sensitive to environmental disturbances, particularly to variations of ambient pressure and temperature [79]. For instance, the laser cavity frequency ν_{ec} depends on temperature according to

$$\frac{d\nu_{\mathrm{ec}}}{dT} \approx -\nu_{\mathrm{ec}}\kappa_{\mathrm{B}}, \tag{3.1}$$

where κ_{B} is the thermal expansion coefficient of the laser body material. If e.g. aluminum (Al 6063) is used for constructing the laser cavity, the thermal sensitivity of the laser can be as high as 11 GHz/K, thus making the laser prone to mode hopping. Typically air comprises a significant part of the optical length of an ECDL cavity, and any variations of the air refractive index shift the laser frequency. Assuming the humidity and composition of the air to remain constant, the frequency shifts as a function of the cavity air pressure and temperature for the 633-nm laser are -109 MHz/hPa and +354 MHz/K, respectively.

Temperature of a diode laser is easy to stabilize using a Peltier element, and in a compact ECDL the same method can be used to compensate, to some extent, the thermal variations of the cavity, too. In addition to active temperature stabilization, thermal expansion of the 633-nm transmission-grating laser is minimized by proper material selections and compensation structures. Thermal expansion affects also in the direction perpendicular to the optical axis, as it changes the places of the cavity components relative to each other [79]. Such changes are eliminated by the laser structure that is symmetrical relative to the optical axis. The effect of ambient pressure is canceled using a hermetically sealed cover.

To ensure rigid construction and to avoid mechanical resonances, the laser design was kept simple and minimum amount of components was used. For example, only one PZT element is used for fine tuning of the laser cavity frequency. This limits the fine-tuning range to approximately one cavity FSR. In practice, the fine-tuning range was observed to be between 3 to 6 GHz, depending e.g. on the quality of the laser diode AR coating, as well as on the grating adjustment. This is sufficient for most spectroscopic applications. For instance, only a 1-GHz continuous tuning range is needed to sweep over an iodine absorption line. Moreover, coarse wavelength tuning of 14 nm is obtained by adjusting the screws that determine the grating angle relative to the laser beam. Side-mode suppression ratio is better than 35 dB over the entire tuning range.

The high mechanical stability of such transmission-grating laser provides enhanced frequency reproducibility and ensures inherently narrow technical linewidth – the measured 1-s linewidth of the laser is as small as 450 kHz. Also the long-term stability of the laser has been demonstrated to be good: At 1000 s integration time the relative stability of the free running laser is better than 8.4×10^{-9} [Publ. II]. These properties,

combined with the invariant output beam pointing, make the laser design suitable for many applications of metrology and atom optics.

3.2.1. Modulation characteristics

Since the 633-nm transmission-grating laser is used in wavelength modulation spectroscopy, its modulation characteristics are of interest. The laser frequency can be modulated either directly through the injection current or by modulating the external-cavity length with a PZT element. With the used PZT element and driver the -3 dB bandwidth of the feedback loop is limited to below 1 kHz, but in practice modulation frequencies higher than 10 kHz can be used by coupling the modulation inductively to the PZT driving voltage. The 3rd harmonic distortion measured from the frequency change of the laser was confirmed to be below -70 dB compared to the fundamental frequency.

The direct current modulation allows much higher modulation frequencies than what is possible with the PZT. However, the drawback of the current modulation is the high degree of spurious intensity modulation (or residual amplitude modulation, RAM), which is detrimental in absorption spectroscopy as it leads to asymmetries and offset in the signal lines, thus shifting the line centers. Spurious intensity modulation also carries the low-frequency noise to the signal frequency, which degrades the signal-to-noise ratio of the measurement [80,81]. Coupling between the intensity and frequency modulations in a current-modulated diode laser is discussed e.g. in Ref. [82].

The magnitude of the spurious intensity modulation increases linearly with the frequency modulation amplitude as is shown in Fig. 3.5 for the two alternative modulation methods. In some cases the spurious intensity modulation can be reduced by means of optical injection locking. This is discussed separately in chapter 4. With the described transmission-grating laser, the intensity modulation associated with direct current modulation can be suppressed to the level that is normally obtained with PZT modulation, or even below it. The attainable suppression depends, however, on the laser operation conditions and on the injection locking parameters.

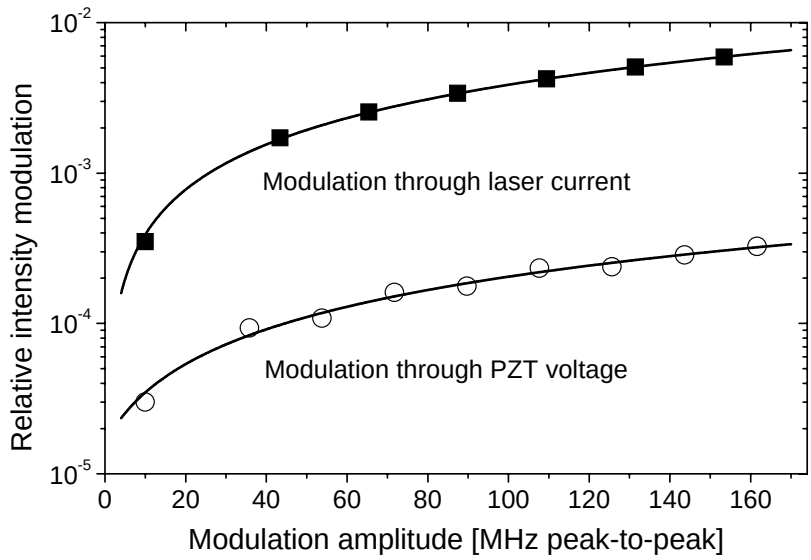

Fig. 3.5 *Spurious intensity modulation of the 633-nm transmission-grating laser. Modulation frequency is 4 kHz.*

4. INJECTION-LOCKED DIODE LASER SYSTEMS

In the following, two practical realizations of laser systems based on injection locking are presented. First, a diode laser spectrometer with good spatial and spectral beam quality is discussed [Publ. II]. In section 4.3, an optical amplifier [Publ. IV] used to facilitate optical frequency comb measurements [Publ. V] is described. Both systems utilize a microlens-coupled diode laser (Circulaser^{TM}, Blue Sky Researcher Inc.) as the slave laser. The primary function of the integrated microlens is to circularize the otherwise elliptical output beam of the laser. In addition, the microlens provides weak optical feedback that is enough to force the laser to operate in a single longitudinal mode (Fig. 2.8). The principle of the microlensed diode laser is described in more detail in Ref. [83].

The related theory of laser injection locking was reviewed in chapter 2. In section 4.2 a theory used to model modulation transfer characteristics of injection-locked diode lasers is outlined. The obtained theoretical results, as well as experimental data, are reported in Publication III.

4.2. Iodine spectrometer

The objective of the work presented in this section was to design and construct an ECDL-based spectrometer that can be used in a frequency stabilization setup to measure, together with a femtosecond optical frequency comb generator [11, Publ. V], the absolute frequencies of various transitions of molecular iodine in the 633-nm region. In length metrology, this is an important spectral region since the He-Ne laser stabilized on the hyperfine spectrum of iodine at 633 nm is one of the most used optical frequency standards recommended by the CIPM for practical realization of the definition of the meter [10]. In practice, one of the hyperfine components of the R(127)11-5 transition of iodine is used. However, the good wavelength tunability of diode lasers allows the use of much stronger transitions in the range 630 to 640 nm. Iodine spectrum in the visible can nowadays be theoretically predicted to better than 10 MHz, and experimental studies have provided a complete atlas of the iodine spectrum in the red part with megahertz accuracy [84,85,86]. To develop better theoretical models and to further improve the frequency standards based on iodine-stabilized lasers, more precise absolute frequency measurements are needed.

Motivated by the need for such measurements, a new iodine spectrometer was developed. To obtain good frequency accuracy, the various sources of frequency shifts (section 2.4.3) in the used saturation spectroscopy configuration have been minimized by optimizing the laser beams for spatial and spectral quality. This is done by injection locking a microlens-coupled diode laser with a nearly Gaussian output beam to the stable transmission-grating diode laser described in section 3.2.

The principle of the constructed iodine spectrometer is shown schematically in Fig. 4.1, and explained in more detail in Publication II. The output of the injection-locked, microlens-coupled diode laser is directed as a pump beam for saturation spectroscopy in the iodine cell. A mirror reflects the pump beam back as a probe beam, and a quarter-wave plate changes the beam polarization so that the output of the setup is obtained from the PBS 2. Another polarizing beam splitter (PBS 3) is needed to get a small part of the output beam to the photodetector (PD 1), which is used for frequency locking. The standard third-harmonic technique explained in section 2.4.2 is used to detect the Doppler-free iodine spectrum, and to lock the laser frequency to the hyperfine components.

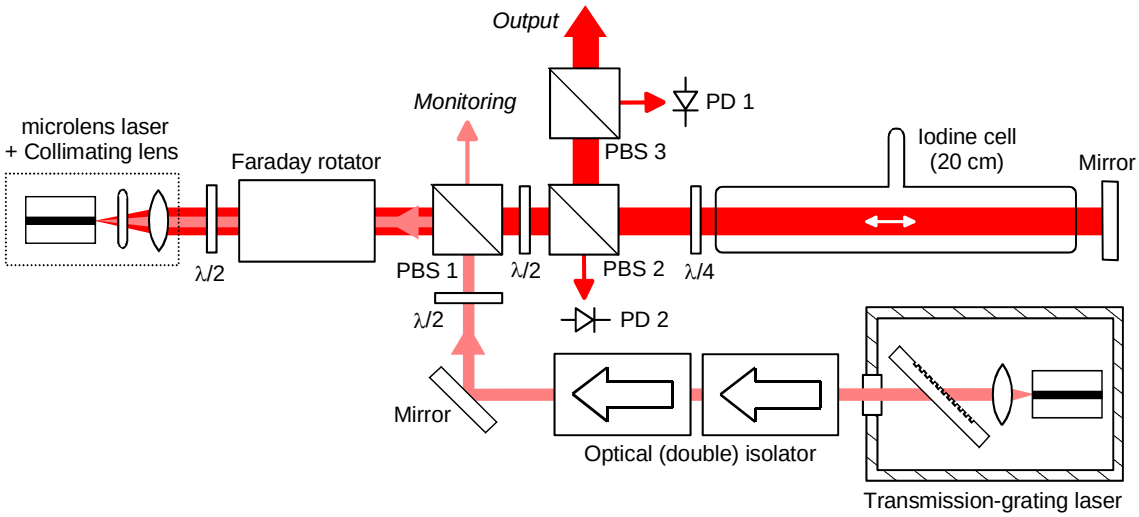

Fig. 4.1 *Principle of the constructed iodine spectrometer [Publ. II]. Abbreviations: PD – photodiode, PBS – polarizing beam splitter, λ/2 – half-wave plate, λ/4 – quarter wave plate.*

The detailed characteristics of the spectrometer are demonstrated in Publication II. The main advantages of the new design are as follows:

- The spectral properties of the system are fully determined by the transmission-grating laser with enhanced frequency stability and reproducibility. The practical (1-s) linewidth of the laser is 450 kHz, which is narrow compared to the iodine hyperfine components.
- Independently of the transmission-grating laser, also the spatial quality of the laser beams used in spectroscopy can be optimized for good frequency accuracy. In the reported system, the beam quality is determined by the microlens-coupled diode laser, which has a circular and nearly Gaussian beam profile.
- The injection-locking scheme reduces the adverse effects of optical feedback [8]. This e.g. allows perfectly collinear alignment of the pump and probe beams, and minimizes the related frequency shifts.
- Due to the good intensity stability of the microlensed laser the frequency instabilities arising from the iodine power shift are very small. These instabilities can be further suppressed using active intensity stabilization.

Moreover, in the injection-locking scheme the frequency of the transmission-grating laser can be modulated simply through injection current, thus allowing much higher modulation frequency than with the conventional PZT modulation. This is because the injection-locking scheme can suppress the problematic spurious intensity modulation, which is typically high for direct current modulation. To get more quantitative information on this phenomenon, a detailed study of modulation transfer properties of injection-locked diode lasers was performed [Publ. III]. This study and its results are summarized in the following section.

4.3. Modulation transfer in diode laser injection locking

Although the suppression of spurious intensity modulation is just one of the benefits of the spectrometer design utilizing diode laser injection locking, it is an interesting and useful feature. The same technique has been previously used in this particular purpose,

namely in suppression of intensity modulation, in FM spectroscopy on rubidium [87]. In addition, diode laser injection-locking has been extensively studied in view of optical communications. For instance, synchronization of a local oscillator for use in coherent transmission systems, enhancement of modulation bandwidth, reduction of nonlinear distortion, and reduction of frequency chirping of modulated injection-locked diode lasers have been demonstrated. These applications, however, are based on direct modulation of an injection-locked laser while the master laser is unmodulated. Recently, there has been research also on systems where the master laser frequency or intensity is modulated and the modulation is transferred to the slave laser, which is injection locked to the master laser. The recent studies include theoretical models of the intensity modulation (IM) and frequency modulation (FM) transfer properties of injection-locked diode lasers [88,49,89] but also experimental data on the dependence of these phenomena on injection ratio and on modulation frequency have been reported [89].

However, the papers published so far do not cover all the aspects that are important e.g. in applications of spectroscopy. Therefore, the transfer of IM and FM in diode laser injection locking was experimentally and theoretically studied for various injection locking conditions. In particular, the dynamic behavior of the master-slave system as a function of frequency detuning was considered. As the main motivation is to use the results for wavelength modulation spectroscopy on iodine, the experimental work only covers the frequency range below 50 kHz. The theoretical analysis is valid also for high modulation frequencies. The results of the research are given in Publication III. In the following, the theoretical model is explained in more detail.

It can be intuitively understood that the output frequency and spectral properties of an injection-locked slave laser are determined by the master laser, while the output power is essentially insensitive to small variations of the master laser intensity. Thus it can be expected that frequency modulation is transferred in injection locking, while intensity modulation can be suppressed. However, using the following analysis it can be shown that these effects depend strongly on the injection locking parameters and e.g. the conversion of master FM to slave IM can play an important role in actual systems.

The analysis utilizes the rate equations, which are recalled below for an injection-locked diode laser

$$\frac{dS(t)}{dt} = \left[G_0\left(N(t) - N_{th}\right) + 2FSR\sqrt{\frac{S_{inj}(t)}{S(t)}}\cos\left(\phi_{inj}(t) - \phi(t)\right)\right] S(t) \tag{4.1.a}$$

$$\frac{d\phi(t)}{dt} = \frac{\alpha}{2} G_0\left(N(t) - N_{th}\right) - 2\pi\Delta f + FSR\sqrt{\frac{S_{inj}(t)}{S(t)}}\sin\left(\phi_{inj}(t) - \phi(t)\right) \tag{4.1.b}$$

$$\frac{dN(t)}{dt} = \frac{I(t)}{e} - \frac{N(t)}{\tau_N} - G_0\left(N(t) - N_{tr}\right). \tag{4.1.c}$$

$S(t)$, $\phi(t)$, and $N(t)$ are the photon number, the phase, and the carrier number inside the slave laser cavity, respectively. Parameter G_0 is the gain coefficient, α is the linewidth enhancement factor, N_{tr} is the carrier number at transparency, and N_{th} is the carrier number at threshold of the free-running slave laser. Parameter $I(t)$ denotes the slave laser bias current, e is the electron charge, and τ_N is the carrier lifetime. The injection rate is proportional to the slave laser free spectral range, FSR. The frequency detuning between the master and slave lasers is given by $\Delta f = \nu_{inj} - \nu_s$, where ν_{inj} denotes the master frequency and ν_s is the unperturbed cavity frequency of the slave laser. The

phase of the injected field is $\phi_{\mathrm{inj}}(t)$, and the number of injected photons inside the slave laser cavity is $S_{\mathrm{inj}}(t)$.

First, the stationary state of the slave laser operating point is solved by setting the time derivatives in (4.1.a) – (4.1.c) to zero. Especially, the steady-state phase difference between the master and slave can be expressed in terms of frequency detuning as

$$\phi_{inj} - \phi = \arcsin\left[\frac{2\pi\Delta f}{FSR\sqrt{\frac{S_{inj}}{S}}\sqrt{1+\alpha^2}}\right] + \arctan(\alpha)\,. \tag{4.2}$$

Also the slave laser photon number S and carrier density N depend on the master-slave frequency detuning Δf. However, to simplify the calculations, these parameters are solved only for one value of detuning and assumed to be constant within the entire locking range (if only other parameters remain unchanged). This approximation was confirmed to be valid in the considered operating conditions.

Dynamic properties of the laser around its stationary state can be studied by following a commonly used procedure to add small modulation terms to the stationary values [51]. If f_{mod} ($= \omega_{\mathrm{mod}}/2\pi$) denotes the modulation frequency, the perturbed variables are given by

$$S_{inj}(t) = S_{inj} + \Delta S_{inj} e^{\mathrm{j}\omega_{\mathrm{mod}}t}, \quad \phi_{inj}(t) = \phi_{inj} + \Delta\phi_{inj} e^{\mathrm{j}\omega_{\mathrm{mod}}t}, \tag{4.3}$$

$$S(t) = S + \Delta S e^{\mathrm{j}\omega_{\mathrm{mod}}t}, \quad \phi(t) = \phi + \Delta\phi e^{\mathrm{j}\omega_{\mathrm{mod}}t}, \quad N(t) = N + \Delta N e^{\mathrm{j}\omega_{\mathrm{mod}}t}. \tag{4.4}$$

These are inserted into the rate equations (4.1) that are then expanded into series. The following approximations (first order Maclaurin expansion) are used:

$$\sqrt{(S+\Delta S e^{\mathrm{j}\omega_{\mathrm{mod}}t})(S_{inj}+\Delta S_{inj} e^{\mathrm{j}\omega_{\mathrm{mod}}t})} \approx \sqrt{SS_{inj}} + \frac{S_{inj}\Delta S + S\Delta S_{inj}}{\sqrt{4SS_{inj}}} e^{\mathrm{j}\omega_{\mathrm{mod}}t} \tag{4.5}$$

$$\cos\left(\left(\phi_{inj}-\phi\right)+\left(\Delta\phi_{inj}-\Delta\phi\right)e^{\mathrm{j}\omega_{\mathrm{mod}}t}\right) \approx \cos\left(\phi_{inj}-\phi\right) - \sin\left(\phi_{inj}-\phi\right)\cdot\left(\Delta\phi_{inj}-\Delta\phi\right)e^{\mathrm{j}\omega_{\mathrm{mod}}t} \tag{4.6}$$

$$\sin\left(\left(\phi_{inj}-\phi\right)+\left(\Delta\phi_{inj}-\Delta\phi\right)e^{\mathrm{j}\omega_{\mathrm{mod}}t}\right) \approx \sin\left(\phi_{inj}-\phi\right) + \cos\left(\phi_{inj}-\phi\right)\cdot\left(\Delta\phi_{inj}-\Delta\phi\right)e^{\mathrm{j}\omega_{\mathrm{mod}}t} \tag{4.7}$$

$$\sqrt{\frac{S_{inj}+\Delta S_{inj} e^{\mathrm{j}\omega_{\mathrm{mod}}t}}{S+\Delta S e^{\mathrm{j}\omega_{\mathrm{mod}}t}}} \approx \sqrt{\frac{S_{inj}}{S}} + \frac{S\Delta S_{inj} - S_{inj}\Delta S}{\sqrt{4S^3 S_{inj}}} e^{\mathrm{j}\omega_{\mathrm{mod}}t}\,. \tag{4.8}$$

Considering the small-signal modulation terms only, the equation for photon-number can be written as

$$\left(\mathrm{j}\omega_{\mathrm{mod}} - G_0(N_{tr}-N_{th}) - FSR\cos(\phi_{inj}-\phi)\sqrt{\frac{S_{inj}}{S}}\right)\cdot\Delta S - 2FSR\sqrt{SS_{inj}}\sin(\phi_{inj}-\phi)\cdot\Delta\phi - G_0 S\cdot\Delta N$$

$$= FSR\cos(\phi_{inj}-\phi)\sqrt{\frac{S_{inj}}{S}}\cdot\Delta S_{inj} - 2FSR\sqrt{SS_{inj}}\sin(\phi_{inj}-\phi)\cdot\Delta\phi_{inj}$$

After following the same procedure for the phase and carrier-number equations, the solution can be presented in matrix form

$$\left(\mathrm{j}\omega_{\mathrm{mod}}\mathbf{I}-\mathbf{M}\right)\begin{bmatrix}\Delta S\\ \Delta\phi\\ \Delta N\end{bmatrix}=\mathbf{N}\begin{bmatrix}\Delta S_{inj}\\ \Delta\phi_{inj}\\ 0\end{bmatrix}, \tag{4.9}$$

where **I** is the identity matrix, and matrices **M** and **N** are expressed as follows:

$$\mathbf{M}=\begin{bmatrix} G_0\left(N-N_{th}\right)+FSR\sqrt{\frac{S_{inj}}{S}}\cos(\phi_{inj}-\phi) & 2FSR\sqrt{S_{inj}S}\sin(\phi_{inj}-\phi) & G_0S \\ -\frac{1}{2}FSR\sqrt{\frac{S_{inj}}{S^3}}\sin(\phi_{inj}-\phi) & -FSR\sqrt{\frac{S_{inj}}{S}}\cos(\phi_{inj}-\phi) & \frac{\alpha}{2}G_0 \\ -G_0\left(N-N_{tr}\right) & 0 & -\frac{1}{\tau_N}-G_0S \end{bmatrix},$$

$$\mathbf{N}=\begin{bmatrix} FSR\sqrt{\frac{S}{S_{inj}}}\cos(\phi_{inj}-\phi) & -2FSR\sqrt{S_{inj}S}\sin(\phi_{inj}-\phi) & 0 \\ \frac{1}{2}\frac{FSR}{\sqrt{S_{inj}S}}\sin(\phi_{inj}-\phi) & FSR\sqrt{\frac{S_{inj}}{S}}\cos(\phi_{inj}-\phi) & 0 \\ 0 & 0 & 0 \end{bmatrix}. \tag{4.10 \& 4.11}$$

The matrix equation (4.9) allows us to calculate how the modulation of the master laser photon number or phase is converted to modulation of the slave laser. For example, transfer efficiency of the intensity modulation index is obtained as $(\Delta S/S)/(\Delta S_{\mathrm{inj}}/S_{\mathrm{inj}})$. All the theoretical results reported in Publication III have been calculated numerically using Eq. (4.9).

The preceding derivation was made for an injection-locking system where the master laser photon number and phase are modulated. If a directly modulated, injection-locked diode laser is considered instead, the solution must be modified as follows: The left side of Eq. (4.9) remains the same but the right side of the equation is replaced with a vector that contains the driving terms for the slave laser modulation. In other words, the matrix **N** accounts for the effect of modulated optical injection. In both cases the system can be checked for dynamical stability by ensuring that the eigenvalues of the characteristic matrix **M** are located in the left half of the complex plane.

Simulated and experimental results for the system described in section 4.1 are given in Publication III. The most important conclusions of the study can be summarized as follows:

- Within the stable locking range, master laser FM is fully transferred to the injection-locked slave laser. This, as well as the other results, holds for all modulation frequencies that are clearly smaller than the slave laser relaxation oscillation frequency. The relaxation oscillation frequency depends on the slave laser bias level (Eq. 2.12) and can also be increased for high levels of optical injection. Typically the relaxation oscillation frequency is a few GHz or more.
- Master laser IM is suppressed in the slave laser. Suppression is higher the smaller the injection ratio. Moreover, the level of IM suppression is strongly

affected by the master-slave detuning. Also the slave laser internal parameters and bias level affect.

- Master laser FM is converted to slave laser IM. Again, the conversion efficiency depends on the master-slave detuning, as well as on the slave laser parameters and bias level. In particular, the amount of generated IM is directly proportional to the frequency modulation amplitude. On the other hand, the effect of injection ratio is small.
- Considering a system similar to the one described in section 4.1 the most important observation is that, if the master laser IM index is initially small (e.g. with PZT-modulation) the FM-to-IM conversion can lead to enhancement of the spurious intensity modulation in the injection-locked slave laser. However, if the master laser IM index is relatively large (as in the case of direct current modulation) suppression of spurious intensity modulation can be obtained by means of injection locking.

Altogether, the theoretical results are in good agreement with the experimental observations. The only significant discrepancy, different extent of the stable locking range is most probably due to the microlens-coupled diode laser used in the experiments. The small optical feedback from the microlens substantially modifies the diode laser gain profile (see Fig. 2.8) and this effect was not taken into account in the calculations. Both the optical feedback and existence of longitudinal side modes are known to affect the injection locking condition [8,53].

4.4. Optical amplifier

One of the most common uses of optical injection locking is to amplify laser output power. As a part of this thesis, an optical amplifier operating at the 633-nm wavelength band has been realized using the injection-locking method. The work is motivated by the increasing need for absolute frequency measurements of iodine-stabilized He-Ne lasers as the emerging of femtosecond frequency comb technology has made such measurements accessible to many national standard institutes and research laboratories.

Iodine-stabilized He-Ne ($HeNe/I_2$) laser at 633 nm is the most widely used optical frequency standard for the practical realization of the definition of the metre [10], and commonly used e.g. in frequency calibration of lasers used in length measurements and gravimeters. To use a laser as a frequency standard, its absolute frequency must be determined. At present the most convenient way to do this is to perform a beat-frequency comparison with an optical femtosecond frequency comb [11]. Unfortunately, however, the frequency comb measurement of the $HeNe/I_2$ laser is impeded due to its low (< 100 μW) output power. The weak and frequency-dithered output is inadequate to produce sufficient signal-to-noise ratio (SNR) for reliable frequency counting. Until now, the problem has been solved e.g. by using a transfer laser [90,91] or by measuring the frequency of a high-power He-Ne laser phase-locked to the iodine-stabilized He-Ne laser under study [92].

The new approach presented in Publication IV relies on optical amplification of the laser power to the level required in the measurement. The amplification is made by injection locking a microlens-coupled diode laser to the laser to be measured (Fig. 4.2). The injection-locking method provides a simple and inexpensive way to facilitate absolute frequency measurements of $HeNe/I_2$ lasers. The same setup could be useful

also in other applications requiring relatively high laser powers, such as in laser interferometry.

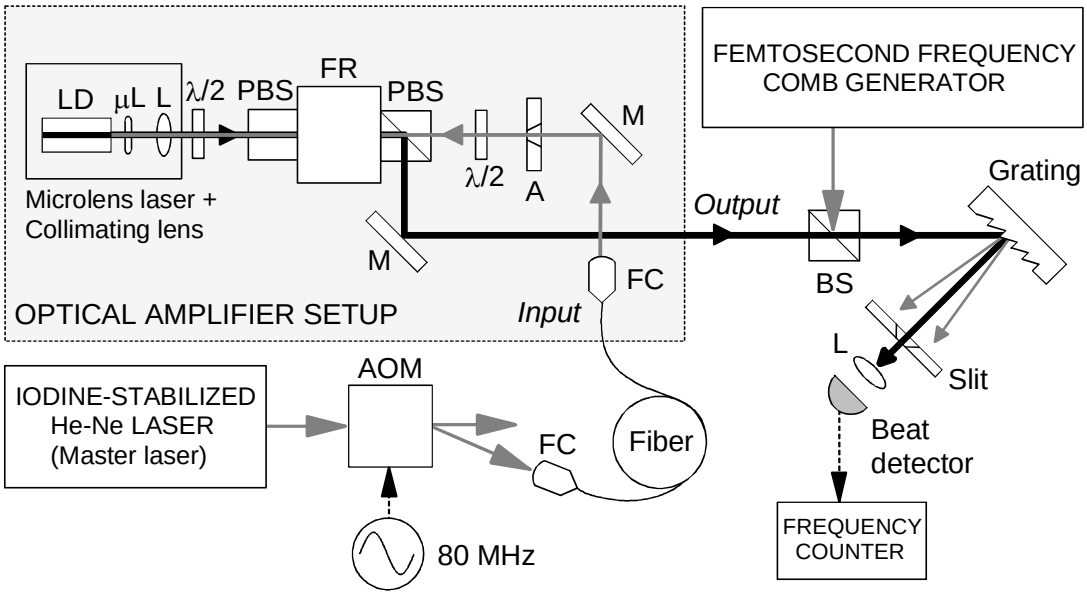

Fig. 4.2 *Principle of the optical amplifier setup operating in the 633-nm wavelength region [Publ. IV]. Also the use in absolute frequency measurements together with an optical frequency comb generator is schematically shown. Abbreviations: A – aperture, AOM – acousto-optic modulator, BS – beamsplitter, FC – fiber coupler, FR – Faraday rotator, L – lens, λ/2 – half-wave plate, LD – laser diode, M – mirror, μL – microlens, and PBS – polarizing beamsplitter.*

Careful characterization of the constructed amplifier has been performed and reported in Publication IV. Reliable long-term operation in normal laboratory conditions has been demonstrated and the amplifier's effect on the results of actual frequency comb measurements has been shown to be negligible. The reported data allows other laboratories to directly use similar approach without need for laborious characterization measurements of their amplifier setups. The results of the absolute frequency determination of MRI3 HeNe/I_2 laser (and of a Nd:YAG/I_2 laser) are presented in Publication V, which also outlines the MIKES frequency comb generator used in the measurements. A brief discussion of the femtosecond frequency comb technology in general is given in the following chapter.

5. OPTICAL FREQUENCY COMB

Optical frequency standards are essentially lasers that are stabilized on molecular, atomic, or ionic transitions. Compared to microwave frequency standards, the optical standards offer potentially much better frequency stability due to their higher operating frequencies [93]. While the microwave frequencies can be directly counted up to the order of 100 GHz, the measurement of absolute optical frequencies (hundreds of THz) is much more challenging. However, the establishment of an optical frequency standard requires that the absolute frequency of the used transition must be measured relative to the primary frequency standard, which is based on the 9.2-GHz cesium hyperfine transition. That is to say, for an absolute frequency measurement in the optical region a phase coherent link to the microwave frequencies is needed.

Previously, due to the laborious nature of the optical domain frequency measurements using frequency chains, there were only few optical transitions that were known relative to the primary standard and could be used as references for accurate frequency measurements in the optical region. At the end of the 1990s the bridging of the optical and microwave domains was remarkably simplified by the demonstration of the full-octave optical frequency comb generator [11,94] that allows direct absolute measurement of any frequency within the comb range. Nowadays, this technology is used in many laboratories to measure e.g. fundamental constants [95,96], lasers stabilized on gas-cell absorbers [90-92] or trapped and cooled ions [97] or atoms [98]. Optical frequency standards and measurements are discussed e.g. in references [93,99].

In generation of the octave-spanning optical frequency combs, Kerr-lens mode-locked Ti:sapphire (Ti:S) lasers are most often used [99]. The Ti:S wavelength is typically centered near 800 nm, and the gain bandwidth is very large, approximately from 700 to 1000 nm. Such a wide gain band makes it possible to generate ultrashort laser pulses of ~ 5 ps [100]. Usual repetition rates for the Ti:S lasers are from tens of MHz to a few GHz, depending on the cavity round-trip time. By adjusting the laser cavity length the repetition rate can be slightly varied.

The octave spanning spectrum can be obtained with a mode-locked femtosecond (Ti:S) laser using two different approaches: direct broadband operation [100,101], or spectral broadening of the laser output in a highly nonlinear microstructured fiber [11]. The latter approach is more common and is also used in the MIKES frequency comb generator described in Publication V. Microstructured fiber consists of a silica core with small diameter (1...5 μm), which is surrounded by air holes. The dispersion properties of the fiber can be designed so that temporal broadening of the Ti:S laser pulses in the fiber is minimized. This ensures that the nonlinear interaction is efficient over a long distance, thus leading to significant spectral broadening. An example of a Ti:S laser spectrum broadened in a microstructured fiber is shown in Fig. 5.1.

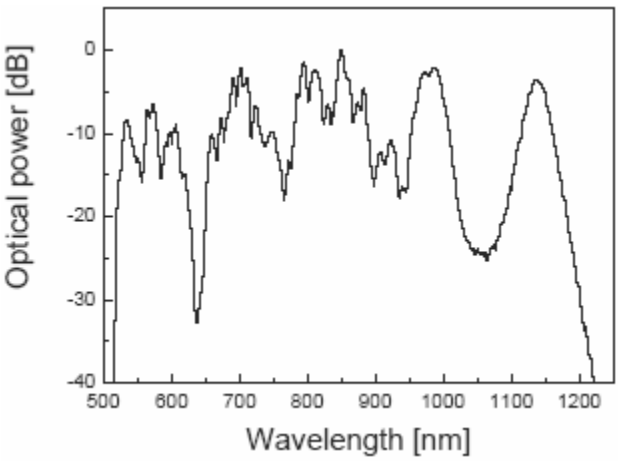

Fig. 5.1 *Typical envelope spectrum of the MIKES frequency comb generator. Highest peak is normalized to 0 dB. The spectrum can be optimized for each wavelength to be measured. Figure reproduced from Publication V.*

The frequency spectrum of Fig. 5.1 is measured using an optical spectrum analyzer that has a resolution far from sufficient for resolving the actual comb structure, which is illustrated in Fig. 5.2. The spacing of the comb lines is the same as the repetition frequency f_{rep} of the Ti:S laser. To use the comb for frequency measurements, the absolute position and spacing of its lines must be known. Since the repetition rate f_{rep} is determined by the laser, it is known. To determine the comb position, or the offset frequency f_o, so-called self-referencing technique is often used. The principle of this technique is schematically shown in Fig. 5.2. The comb component with the mode number n and optical frequency $\nu_1 = nf_{rep} + f_o$ from the red part of the spectra is frequency doubled to a frequency $2\nu_1 = 2(nf_{rep} + f_o)$. If the comb extends over an optical octave the doubled frequency $2\nu_1$ can be compared in a beat measurement with the comb component $\nu_2 = 2nf_{rep} + f_o$ in the blue part of the spectra. The beat note between the frequency doubled mode and the mode $2n$ directly gives the value of the offset frequency since $2(nf_{rep} + f_o) - 2nf_{rep} + f_o = f_o$.

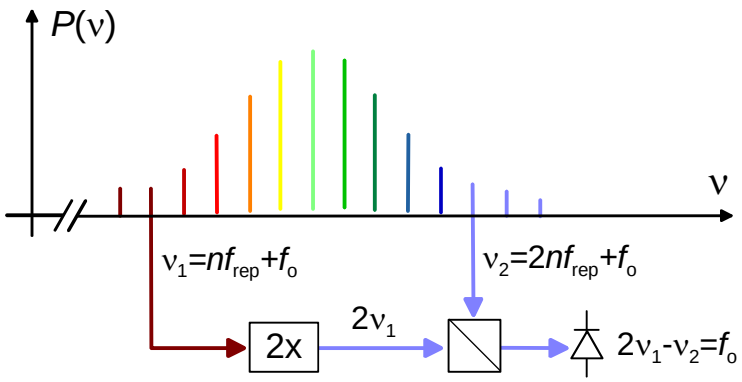

Fig. 5.2 *Self-referencing the octave-spanning frequency comb produces a beat note at offset frequency f_o.*

In practice, the repetition rate and the offset frequency are phase locked to an atomic clock by controlling the Ti:S cavity length and pump power, thereby providing an absolutely known line spectrum. The absolute frequency of a laser can now be measured by a direct beat-frequency comparison against the nearby line of the comb. The multiple

integer (mode number) *n* can be determined e.g. from a coarse measurement with a wavemeter. However, normally this is not needed as many laser frequencies are already known at a level much less than the comb spacing.

A more detailed description of the MIKES frequency comb generator, together with the results of absolute frequency measurements for two iodine-stabilized lasers are reported in Publication V. All the measured frequencies are in good agreement with previous results and the CIPM recommended values. For the most important $^{127}I_2$ transitions, R(56)32-0 and R(127)11-5, the differences are less than 0.2 kHz with respect to the CIPM recommendations.

6. CONCLUSION

In this thesis, techniques based on optical feedback and optical injection have been used and studied for improving characteristics of semiconductor diode lasers. The main applications of the research are in metrology, but many of the results are useful also in optical communications and atom optics.

Many of the present applications in spectroscopy, for example, require stable laser sources with narrow linewidth and good wavelength tunability. External-cavity diode lasers are commonly used in such applications, and also in this work two external-cavity diode lasers have been built and characterized. Both lasers utilize transmission grating as a dispersive optical feedback element. The main advantage of the transmission-grating geometry is invariant output beam pointing, which is useful e.g. in coupling light into an optical fiber, and essentially important in applications like spectroscopy and laser injection locking. Transmission grating has been shown to give stable and reliable operation over the entire gain spectra of the used diode lasers. In telecommunication wavelengths, a tuning range as wide as 128 nm has been demonstrated. In addition, a new transmission-grating laser design with very good passive stability and narrow linewidth has been presented.

In length metrology, one of the most important spectral regions is the visible red near 633 nm wavelength. Iodine-stabilized He-Ne (HeNe/I_2) laser stabilized on the hyperfine spectrum of the R(127)11-5 transition is one of the most used optical frequency standards recommended by the CIPM for practical realization of the definition of the meter. In addition to the R(127)11-5 transition, there are also much stronger transitions in the wavelength range 630 to 640 nm, which makes it attractive to develop new frequency standards based on tunable diode lasers. Both to improve already existing optical frequency standards and to develop new ones, precise absolute frequency measurements of the used iodine transitions are needed. At present, such measurements can be performed using an optical femtosecond frequency comb generator.

In this thesis, two different setups for absolute frequency measurements with the optical frequency comb generator have been developed. Both realizations are based on diode laser injection locking, i.e. on a master-slave system where light from a master laser is injected into a slave laser, which then copies the spectral properties of the master laser. To facilitate the absolute frequency measurements of the HeNe/I_2 laser, an optical amplifier has been constructed. The output power of the iodine-stabilized He-Ne laser as such is too low for direct frequency comb measurements, and the amplifier developed here provides a convenient and inexpensive all-optical way to raise the laser output to the required level. The amplifier can be reliably operated over several hours with very low phase noise, and it has been successfully used in absolute frequency determination of an iodine-stabilized He-Ne laser. The reported system description and characterization allows other laboratories to directly implement similar approach to their measurement setups.

As another application of diode laser injection locking, a laser spectrometer for absolute frequency determination of various iodine transitions in the vicinity of 633 nm has been realized. The new spectrometer design has been made particularly for good frequency accuracy and reproducibility, and it combines good beam quality of a microlens-coupled diode laser with high spectral quality of the transmission-grating laser. The spectrometer uses wavelength modulation technique for locking the laser frequency to an iodine hyperfine component. Since the modulation properties of the laser are

important for the overall performance of the spectrometer, a detailed study of systems where the master laser is modulated and the modulation is transferred to the injection-locked slave laser was performed. In particular, suppression of intensity modulation (IM) and reproduction of frequency modulation (FM) have been considered, for the first time, in terms of master-slave detuning. Moreover, the importance of FM-to-IM conversion in injection-locked diode lasers has been pointed out. In addition to spectroscopy, the results are useful in optical communications.

REFERENCES

1. C.E. Wieman and L. Hollberg, “Using diode lasers for atomic physics,” Rev. Sci. Instrum. **62**, pp. 1-20 (1991).

2. L. Ricci, M. Weidemüller, T. Esslinger, A. Hemmerich, C. Zimmermann, V. Vuletic, W. König, and T.W. Hänch, “A compact grating-stabilized diode laser system for atomic physics,“ Opt. Commun. **117**, 541-549 (1995).

3. G.H.M. van Tartwijk and D. Lenstra, ”Semiconductor lasers with optical injection and feedback,” Quantum and Semiclasss. Opt. **7**, pp. 87-143 (1995).

4. E.J. Bochove, “Theory of modulation of an injection-locked semiconductor diode laser with applications to laser characterization,” J. Opt. Soc. Am. B **14**, pp. 2381-2391 (1997).

5 . T. B. Simpson, J. M. Liu, and A. Gavrielides, “Bandwidth enhancement and broadband noise reduction in injection-locked semiconductor lasers,” IEEE Photon. Technol. Lett. **7**, pp. 709-711 (1995).

6. J. Wang, M. K. Haldar, L. Li, and F. V. C. Mendis, “Enhancement of modulation bandwidth of laser diodes by injection locking,” IEEE Photon. Technol. Lett. **8**, pp. 34-36 (1996).

7. N.A. Olsson, H. Temkin, R. A. Logan, L. F. Johnson, G. J.Dolan, J. P. Van der Ziel, and J. C. Campbell, “Chirp-free transmission over 82.5 km of single mode fibers at 2 Gbit/s with injection locked DFB semiconductor lasers,” J. Lightwave Technol. **LT-3**, 63-67 (1985).

8. J.S. Lawrence and D.M. Kane, ” Injection locking suppression of coherence collapse in a diode laser with optical feedback,” Opt. Commun. **167**, pp. 273-282 (1999).

9. M. Merimaa, H. Talvitie, P. Laakkonen, M. Kuittinen, I. Tittonen, and E. Ikonen, ”Compact external-cavity diode laser with a novel transmission geometry,” Opt. Commun. **174**, pp. 175-180 (2000).

10. T. J. Quinn, “Practical realization of the definition of the metre, including recommended radiations of other optical frequency standards (2001),” Metrologia **40**, pp. 103-133 (2003) + revisions by the Working Group on the Mise en Pratique (MEP2003).

11. S.A. Diddams, D.J. Jones, J. Ye, S.T. Cundiff, J.L. Hall, J.K. Ranka, R.S. Windeler, R. Holzwarth, T. Udem, and T.W. Hänch, “Direct link between microwave and optical frequencies with a 300 THz femtosecond laser comb,” Phys. Rev. Lett. **84**, p. 5102 - 5105 (2000).

12. M. Bagley, R. Wyatt, D.J. Elton, H.J. Wickes, P.C. Spurdens, C.P. Seltzer, D.M. Cooper, W.J. Devlin, “242 nm continuous tuning from a GRIN-SC-MQW-BH InGaAsP laser in an extended cavity,” Electron. Lett. **26**, pp. 267-269 (1990).

13. H. Tabuchi and H. Ishikawa, ”External grating tunable MQW laser with wide tuning range of 240 nm,” Electron. Lett. **26**, pp. 742-743 (1990).

14. T. Ikegami, S. Sudo, and Y. Sakai, Frequency stabilization of semiconductor laser diodes, Artech House, Boston, USA (1995).

13. J. Singh, Semiconductor optoelectronics – physics and technology, McGraw-Hill, Inc., Singapore (1995).

16. W.W. Chow and S.W. Koch, Semiconductor-laser fundamentals – Physics of the gain materials, Springer-Verlag Berlin Heidelberg, Germany (1999).

17. C.H. Henry, “Theory of the linewidth of semiconductor lasers,” IEEE J. Quantum Electron. **18**, pp. 259-264 (1982).

18. M. Lax, “Fluctuations from the nonequilibrium steady state”, Rev. Mod. Phys. **32**, pp. 25-64 (1960).

19. W. Demtröder, Laser spectroscopy, Springer-Verlag Berlin Heidelberg, Germany (1996).

20. S. Balle, ”Effective two-level-model with asymmetric gain for laser diodes,” Opt. Commun. **119**, pp. 227-235 (1995).

21. J. Buus, Single frequency semiconductor lasers, SPIE – The international Society for Optical Engineering, Bellingham (1991).

22. M. Osinski and J. Buus, “Linewidth broadening factor in semiconductor lasers – an overview,” IEEE J. Quantum Electron. **23**, pp. 9-29 (1987).

23. B.O. Nilsson, ”Noise mechanisms in laser diodes,” IEEE Transactions on Electron Devices **41**, pp. 2139-2150 (1994).

24. L.B. Mercer, “1/f frequency noise effects on self-heterodyne linewidth measurements,” J. Lightwave Technol. **9**, pp. 485-493 (1991).

25. L. Hsu, A. Mooradian, and R.L. Aggarwal, “Spectral linewidth of free-running continuous-wave single-frequency external-cavity quantum-well InGaAs/AlGaAs diode laser,” Opt. Lett. **20**, pp. 1788-1790 (1995).

26. K. Kikuchi, “Effect of 1/f-type FM noise on semiconductor laser linewidth residual in high-power limit,” IEEE J. Quantum Electron. **25**, pp. 684-688 (1989).

27. A. Dandridge and H.F. Taylor, “Correlation of low-frequency intensity and frequency fluctuations in GaAlAs lasers,” IEEE J. Quantum Electron. **18**, pp. 1738-1750 (1982).

28. M. Ohtsu, H. Fukada, T. Tako, H. Tsuchida, “Estimation of the ultimate frequency stability of semiconductor lasers,” Jpn. J. Appl. Phys. **22**, pp. 1157-1166 (1983).

29. L.D. Turner, K.P. Weber, C.J. Hawthorn, R.E. Scholten, “Frequency noise characterization of narrow linewidth diode lasers,” Opt. Commun. **201**, pp. 391-397 (2002).

30. M. Kourogi and M. Ohtsu, “Novel optical frequency discriminator for FM noise reduction of semiconductor lasers,” Opt. Commun. **81**, p. 204-208 (1991).

31. D.R. Hjelme, A.R. Michelson, and R.G. Beausoleil, “Semiconductor laser stabilization by external optical feedback,” IEEE J. Quantum Electron. **27**, p. 352 (1991).

32. M. Yousefi, D. Lenstra, and G. Vemuri, “Carrier inversion noise has important influence on the dynamics of a semiconductor laser,” IEEE J. Selected Topics in Quantum Electron. **10**, pp. 955-960 (2004).

33. C. Becher, E. Gehrig, and K.-J. Boller, “Spectrally asymmetric mode correlation and intensity noise in pump-noise-suppressed laser diodes,” Phys. Rev. A **57**, pp. 3952-3960 (1998).

34. J-P. Poizat, T. Chang, O. Ripoll, and P. Grangier, “Spatial quantum noise of laser diodes,” J. Opt. Soc. Am. B **15**, pp. 1757-1761 (1998).

35. K. Petermann, “External optical feedback phenomena in semiconductor lasers,” IEEE J. Selected Topics in Quantum Electron. **1**, pp. 480-489 (1995).

36. F. Favre and D. Le Guen: Electron. Lett. **19**, 663 (1983).

37. F. Wittgrefe, M. D. Hoogerland, and J. P. Woerdman: Meas. Sci. Technol. **2**, 304 (1991).

38. R.W. Tkach and A.R. Chraplyvy, ”Regimes of feedback effects in 1.58m distributed feedback lasers,” J. Lightwave Technol. **4**, pp. 1655-1661 (1986).

39. N. Schunk and K. Petermann, “Numerical analysis of the feedback regimes for a single-mode semiconductor laser with external feedback,” IEEE J. Quantum Electron. **24**, p. 1242-1247 (1988).

40. H. Li, J. Ye, and J.G. McInerney, “Detailed analysis of coherence collapse in semiconductor lasers,” IEEE J. Quantum Electron. **9**, pp. 2421-2432 (1993).

41. K.I. Kallimani and M.J. O’Mahony, “Relative intensity noise for laser diodes with arbitrary amounts of optical feedback,” IEEE J. Quantum Electron. **34**, p. 1438-1446 (1998).

42. Y. Hong, S. Bandyopadhyay, S. Sivaprakasam, P.S. Spencer, and K.A. Shore, “Noise characteristics of a single-mode laser diode subject to strong optical feedback,” J. Lightwave Technol. **20**, pp. 1847-1850 (2002).

43. B. Tromborg, H. Olesen, X. Pan, and S. Saito, ”Transmission line description of optical feedback and injection locking for Fabry-Perot and DFB lasers,” IEEE J. Quantum Electron. **23**, pp. 1875-1889 (1987).

44. R.J. Lang and A. Yariv, ”An exact formulation of couple-mode theory for coupled-cavity lasers,” IEEE J. Quantum Electron. **24**, pp. 66-72 (1988).

45. H. Sun, S. Menhart, and A. Adams, ”Calculation of spectral linewidth reduction of external-cavity strong-feedback semiconductor lasers,” Appl. Opt. **33**, pp. 4771-4775 (1994).

46. P. Zorabedian, W. Trutna, and L. Cutler, ”Bistability in grating-tuned external-cavity semiconductor lasers,” IEEE J. Quantum Electron. **23**, pp. 1855-1860 (1987).

47. M. Houssin, B. Fermigier, and M. Desaintfuscien, ”Simulation of the frequency behavior of external-cavity semiconductor lasers,” IEEE J. Quantum Electron. **39**, pp. 833-837 (2003).

48. Sacher Lasertechnik, Technical note ”Classification of antireflection coatings for diode lasers,” http://data.sacher-laser.com/techdocs/classes.pdf (25.11.2004).

49. M. K. Haldar, J. C. Coetzee, and K. B. Gan, “Optical frequency modulation and intensity modulation suppression in a master–slave semiconductor laser system with direct modulation of the master laser,”IEEE J. Quantum Electron. **41** pp. 280-286 (2005).

50. I. Petitbon, P. Gallion, G. Debarge, and C. Chabran, “Locking bandwidth and relaxation oscillations of an injection-locked semiconductor laser,” IEEE J. Quantum Electron. **24** pp. 148-154 (1988).

51. F. Mogensen, H. Olesen, and G. Jacobsen, “ Locking condition and stability properties for a semiconductor laser with external light injection,“ IEEE J. Quantum Electron. **QE-21**, pp. 784-793 (1985).

52. R. Lang, “Injection locking properties of a semiconductor laser,” IEEE J. Quantum Electron. **18**, pp. 976-983 (1982).

53. Y. Hong and K.A. Shore, “Locking characteristics of a side-mode injected semiconductor laser,” IEEE J. Quantum Electron. **35**, pp. 1713-1717 (1999).

54. S. Kobayashi and T. Kimura, “Injection locking in AlGaAs semiconductor laser,” IEEE J. Quantum Electron. **QE-17**, pp. 681-689 (1981).

55. S. Wieczorek, T.B. Simpson, B. Krauskopf, and D. Lenstra, “Bifurcation transitions in an optically injected diode laser: theory and experiment,” Opt. Commun, **215**, pp. 125-134 (2003).

56. S. Eriksson and Å.M. Lindberg, “Observations on the dynamics of semiconductor lasers subjected to external optical injection,” J. Opt. B: Quantum and Semiclass, Opt. **4**, pp. 149-154 (2002).

57. V.Annovazzi-Lodi, A. Sciré, M. Sorel, and S. Donati, “Dynamic behavior an locking of a semiconductor laser subjected to external injection,” IEEE J. Quantum Electron. **34**, pp. 2350-2357 (1998).

58. S. Fredin-Picard, ”On the hyperfine structure of iodine: 1. How to calculate hyperfine transition energies,” BIPM-90/5 report (1990).

59. M. Gläser, ”Hyperfine components of iodine for optical frequency standards,” PTB-Opt-25 (1987).

60. W-Y. Cheng, L. Chen, T.H. Yoon, J.L. hall, and J. Ye, ”Sub-Doppler molecular-iodine transitions near the dissociation limit (523-498 nm),” Opt. Lett. **27**, pp. 571-573 (2002).

61. A. Titov, I. Malinovsky, and M. Erin, ”Determination of saturation parameter in iodine and precise molecular linewidth measurements in He-Ne/I2 standard at 633 nm,” Opt. Commun. **136**, 327-334 (1997).

62. D.N. Ghosh Roy, F. Bertinetto, B.I. Rebaglia, and P.C. Cresto, ”Effects of iodine saturation dispersion on the 127I2 stabilized He-Ne laser,” J. Appl. Phys. **54**, pp. 531-534 (1983).

63. O. Svelto, Principles of lasers, Plenum Press, New York (1998).

64. A.J. Wallard, “Frequency stabilization of helium-neon laser by saturated absorption in iodine vapor,” J. Phys. E: Scient. Instr. **5**, pp. 926–930 (1972).

65. J. Rutman and F-L. Walls, “Characterization of frequency stability in precision frequency sources,” Proceedings of the IEEE **79**, pp. 952-959 (1991).

66. J. Hu, E. Ikonen, and K. Riski, ”On the nth harmonic locking of the iodine stabilized He-Ne laser,” Opt. Commun. **120**, pp. 65-70 (1995).

67. M. Bisi and F. Bertinetto, ”Frequency reproducibility of He-Ne lasers at $\lambda = 612$ nm using the frequency modulation spectroscopy technique,” Metrologia **34**, pp. 451-457 (1997).

68. M. Merimaa, P. Kokkonen, K. Nyholm, and E. Ikonen, ”A portable laser frequency standard at 633 nm with a compact external-cavity diode laser,” Metrologia **38**, pp. 311-318 (2001).

69. H.R. Simonsen, ”Iodine stabilized extended cavity diode laser at $\lambda = 633$ nm,” IEEE Transactions on Instrumentation and Measurement **46**, pp. 141-144 (1997).

70. P. Kluczynski, J. Gustafsson, A. Lindberg, and O. Axner, “Wavelength modulation absorption spectrometry—an extensive scrutiny of the generation of signals,” Spectrochim. Acta B **56**, pp. 1277–1354 (2001).

71. J.L. Hall and C.J. Bordé, ”Shift and broadening of saturated absorption resonances due to curvature of the laser wave fronts,” Appl. Phys. Lett. **29**, pp. 788-790 (1976).

72. M. Merimaa, H. Talvitie, J. Hu, and E. Ikonen, ”Iodine-stabilized diode laser at 633 nm: effects of optical feedback,” IEEE Transactions on Instrumentation and Measurement **48**, pp. 587-591 (1997).

73. J. Faist, F. Capasso, D. Sivco, C. Sirtori, A.L. Hutchinson, and A.Y. Cho, “Quantum Cascade Laser,” Science, **264**, pp. 553-556 (1994).

74. K Namjou, S Cai, EA Whittaker, J Faist, C Gmachl, “Sensitive absorption spectroscopy with a room-temperature distributed-feedback quantum-cascade laser,” Opt. Lett. **23**, pp. 219-221 (1998).

75. J.D. Berger, Y. Zhang, J.D. Grade, H. Lee, S. Hrinya, and H. Jerman, ”Widely tunable external cavity diode laser based on a MEMS electrostatic rotary actuator,” in Proc. OFC Conf. Exhibit 2, paper TuJ2-T1-3 (2001).

76. C.J. Hawthorn, K.P. Weber, and R.E. Scholten, ”Littrow configuration tunable external cavity diode laser with fixed direction output beam,” Rev. Sci. Instrum. **72**, pp. 4477-4479 (2001).

77. A. Wicht, M. Rudolf, P. Huke, R.-H. Rinkleff, and K. Danzmann, “Grating enhanced external cavity diode laser,” Appl. Phys. B **78**, pp. 137-144 (2004).

78. J. Lazar, O. Cíp, and B. Ruzicka, “The design of a compact and tunable extended-cavity semiconductor laser,” Meas. Sci. Technol. **15**, N6-N9 (2004).

79. H. Talvitie, A. Pietiläinen, H. Ludvigsen, and E. Ikonen, ”Passive frequency and intensity stabilization of extended-cavity diode lasers,” Rev. Sci. Instrum. **68**, pp. 1-7 (1997).

80. D.S. Bomse, A.C. Stanton, and J.A. Silver, ”Frequency modulation and wavelength modulation spectroscopies: comparison of experimental methods using a lead-salt diode laser,” Appl. Opt. **31** pp. 718-731 (1992).

81. M. Gehrtz, G.C. Bjorklund, and E.A. Whittaker, “Quantum-limited laser frequency-modulation spectroscopy,” J. Opt. Soc. Am. B **2**, pp. 1510-1526 (1985).

82. S. Schilt and L. Thévenaz, “Experimental method based on wavelength-modulation spectroscopy for the characterization of semiconductor lasers under direct modulation,” Appl. Opt. **43**, pp. 4446-4453 (2004).

83. H. Talvitie, M. Merimaa, and E. Ikonen, ”Frequency stabilization of a diode laser to Doppler-free spectrum of molecular iodine at 633 nm,” Opt. Commun. **152**, pp. 182-188 (1998).

84. H. Knöckel, B. Bodermann, and E. Tiemann, ”High precision description of the rovibronic structure of the I B-X spectrum,” Eur. Phys. J. D **28**, pp. 199-209 (2004).

85. B. Bodermann, M. Franck, H. Knöckel, and E. Tiemann, ”Iodine atlas as frequency reference online,” in Proc. 16th Colloquium on High Resolution Molecular Spectroscopy, Paper D30, **134** (1999).

86. H. Kato, S. Kasahara, K. Ishikawa, M. Misono, Y. Kimura, J. O’Reilly, H. Kuwano, T. Shimamoto, T. Shimano, C. Fujiwara, M. Ikeuchi, N. Fujita, M.D. Kabira, M. Ushino, R. Takahashi, and Y. Matsunobo, ”Doppler-free high resolution spectral atlas of iodine molecule 15.000 to 19.000 cm^{-1},” Paper M32, 388 (1999).

87. S. Kasapi, S. Lathi, Y. Yamamoto, ”Amplitude-squeezed, frequency-modulated, tunable, diode-laser-based source for sub-shot-noise FM spectroscopy,” Opt. Lett. **22** pp. 478-480 (1997).

88. M. Bhattacharya and T. Chattopadhyay, “A method for generation of optical FM signal through injection locking ,” J. Lightwave Technol. **16**, pp. 656-660 (1998).

89. E. K. Lau and M. C. Wu, ” Amplitude and frequency modulation of the master laser in injection-locked laser systems,” Microwave Photonics MWP'04 (2004) 142.

90. L.-S. Ma, S. Picard, M. Zucco, J.-M. Chartier, L. Robertsson, and R. S. Windeler, "Direct measurement of the absolute frequency of the international reference laser BIPM4," Metrologia **41**, pp. 65-68 (2004).

91. S. N. Lea, W. R. C. Rowley, H. S. Margolis, G. P. Barwood, G. Huang, P. Gill, J.-M. Chartier, and R. S. Windeler, "Absolute frequency measurements of 633nm iodine-stabilized helium–neon lasers," Metrologia **40**, pp. 84-88 (2003).

92. T. H. Yoon, J. Ye, J. L. Hall, and J.-M. Chartier, "Absolute frequency measurement of the iodine-stabilized He-Ne laser at 633 nm," Appl. Phys. B **72**, pp. 221-226 (2001).

93. L. Hollberg, C.W. Oates, E.A. Curtis, E.N. Ivanov, S.A. Diddams, T. Udem, H.G. Robinson, J. C. Bergquist, R. J. Rafac, W. M. Itano, R. E. Drullinger, and D.J. Wineland "Optical frequency standards and measurements," IEEE J. Quantum Electron. **37**, pp. 1502-1513 (2001).

94. D. J. Jones, S. A. Diddams, J. K. Ranka, A. Stentz , R. S. Windeler, J. L. Hall, and S. T. Cundiff, "Carrier-envelope phase control of femtosecond mode-locked lasers and direct optical frequency synthesis," Science **288**, pp. 635-639 (2000).

95. M. Niering, R. Holzwarth, J. Reichert, P. Pokasov, Th. Udem, M. Weitz, T. W. Hänsch, P. Lemonde, G. Santarelli, M. Abgrall, P. Laurent, C. Salomon, and A. Clairon, "Measurement of the hydrogen 1S-2S transition frequency by phase coherent comparison with a microwave cesium fountain clock", Phys. Rev. Lett. **84**, pp. 5496-5499 (2000).

96. M. Fischer, N. Kolachevsky, M. Zimmermann, R. Holzwarth, Th. Udem, T. W. Hänsch, M. Abgrall, J. Grünert, I. Maksimovic, S. Bize, H. Marion, F. Pereira Dos Santos, P. Lemonde, G. Santarelli, P. Laurent, A. Clairon, and C. Salomon, "New limits on the drift of fundamental constants from laboratory measurements", Phys. Rev. Lett. **92**, 230802-1 - 230802-4 (2004).

97. H. S. Margolis, G. P. Barwood, G. Huang, H. A. Klein, S. N. Lea, K. Szymaniec, and P. Gill, "Hertz-Level Measurement ofthe Optical Clock Frequency in a Single 88Sr+ Ion," Science **306**, pp. 1355-1358 (2004).

98. Th. Udem, S. A. Diddams, K.R. Vogel, C.W. Oates, E.A. Curtis, W.D. Lee, W.M. Itano, R.E. Drullinger, J.C. Bergquist, and L. Hollberg, "Absolute frequency measurements of the Hg^+ and Ca optical clock transitions with a femtosecond laser," Phys. Rev. Lett. **86**, pp. 4996-4999 (2001).

99. T. Cundiff, J. Ye, and J.L. Hall, "Optical frequency synthesis based on mode-locked lasers," Rev. Sci. Instrum. **72**, pp. 3749-3771 (2001).

100. Ell, U. Mogner, F.X. Kärtner, J.G. Fujimoto, and E.P. Ippen, "Generation of 5-fs pulses and octave-spanning spectra directly from a Ti:sapphire laser," Opt. Lett. **26**, pp. 373-375 (2001).

101. A. Bartels and H. Kurz, "Generation of a broadband continuum by a Ti:sapphire femtosecond oscillator with a 1-GHz repetition rate," Opt. Lett. **27**, pp. 1839-1841 (2002).

ISBN 951-22-8100-7
ISBN 951-22-8101-5 (PDF)
ISSN 1795-2239
ISSN 1795-4584 (PDF)